Highlights of the manuscript "Temporal variability of the Circumpolar Deep Water inflow onto the Ross Sea continental shelf by Castagno et al.

Ms. Ref. No.: MARSYS-D-16-00002

- Spatial and temporal variability of CDW inflow onto the shelf were characterized.
- Two cores of mCDW intruding over the Ross Sea shelf were detected
- Strong seasonal and interannual variability of mCDW intrusions was observed.
- Variability of the mCDW inflow is tide related.
- Modification of the tidal ellipses orientation before and after 2010 was noticed.

Temporal variability of the Circumpolar Deep Water inflow onto the Ross Sea continental shelf

Pasquale Castagno[a*], Pierpaolo Falco[a], Michael S. Dinniman[b], Giancarlo Spezie[a], Giorgio Budillon[a]

[a]Università degli Studi di Napoli ''Parthenope'', Dipartimento di Scienze e Tecnologie, Napoli, Italy

[b]Center for Coastal Physical Oceanography, Old Dominion University, Norfolk, VA USA – 23529

*Corresponding Author: Pasquale Castagno, Email: pasquale.castagno@uniparthenope.it

Keywords

Cross-shelf exchange; Warm water intrusion; Tidal mixing

Abstract

The intrusion of Circumpolar Deep Water (CDW) is the primary source of heat, salt and nutrients onto Antarctica's continental shelves and plays a major role in the shelf physical and biological processes.

Different studies have analyzed the processes responsible for the transport of CDW across the Ross Sea shelf break, but until now, there are no continuous observations that investigate the timing of the intrusions. Also, few works have focused on the effect of the tides that control these intrusions.

In the Ross Sea, the CDW intrudes onto the shelf in several locations, but mostly along the troughs.

We use hydrographic observations and a mooring placed on the outer shelf in the middle of the Drygalski Trough in order to characterize the spatial and temporal variability of CDW inflow onto the shelf. Our data span from 2004 to the beginning of 2014.

In the Drygalski Trough, the CDW enters as a 150 m thick layer between 250 and 400 m, and moves upward towards the south. At the mooring location, about 50 km from the shelf break, two main CDW cores can be observed: one on the east side of the trough spreading along the west slope of Mawson Bank from about 200 m to the bottom and the other one in the central-west side from 200 m to about 350 m depth.

A signature of this lighter and relatively warm water is detected by the instruments on the mooring at bottom of the Drygalski Trough. The intermittent CDW intrusion at the bottom of the trough is strictly related to the diurnal and spring/neap tidal cycles.

At lower frequency, a seasonal variability of the CDW intrusion is noticed. A strong inflow of CDW is observed every year at the end of December, while the CDW inflow is at its seasonal minimum during the beginning of the austral fall. In addition an interannual variability is also evident. A change of the CDW intrusion before and after 2010 is observed.

1 Introduction

The exchanges of water between the open ocean and the continental shelves around Antarctica play a key role in the global ocean circulation, biogeochemical cycling of carbon and nutrients and the mass balance of the ice sheets.

Cold and dense shelf water leaves the continental shelf in some locations (such as the Ross Sea), ventilating the abyssal oceans and participating in Antarctic Bottom Water

(AABW) formation. AABW is a key component in the global thermohaline circulation (Orsi et al., 1999, 2002; Jacobs, 2004; Johnson, 2008).

Meanwhile, the Circumpolar Deep Water (CDW), a relatively warm and salty, low oxygenated and rich in nutrients water mass, intrudes over the shelf. The inflow of this warm water onto the Antarctic continental shelves has a great influence on the heat, salt and nutrient budget of the coastal ocean and is a potential heat source for the ice shelf basal melt (Rignot and Jacobs, 2002; Pritchard et al., 2012). In addition, the intrusion of CDW has also an important role in AABW formation (Foster and Carmack, 1976; Nicholls et al., 2009; Whitworth and Orsi 2006, Budillon et al. 2011).

Because of the characteristics of the bottom topography, the Western Ross Sea is believed to be a preferable site for CDW onshore intrusions (Dinniman et al., 2003; Klinck and Dinniman, 2010). In particular, they observed that CDW intrudes onto the shelf at sites where the bottom topography changes direction relative to the slope flow.

CDW enters over the shelf near the shelf break and mixes with the Antarctic Slope Front (ASF), a strong, variable boundary between open sea and shelf waters (Jacobs and Giulivi, 2010), characterized by a cold, fresh, V-shaped westward current (Gill 1973).

The mixing of CDW with the Antarctic slope current and the shelf waters over the slope and outer shelf forms a different water mass found on the continental shelf defined as modified Circumpolar Deep Water (mCDW).

The most energetic processes that help the intrusion of CDW over the shelf and contribute to the formation of mCDW through mixing are the tides (Whithworth and Orsi, 2006; Padman et al., 2009). The tidal currents in the Ross Sea are predominantly diurnal and essentially barotropic (Robertson, 2005; Padman et al., 2009). At the shelf break, the tidal currents are associated principally with diurnal topographically trapped waves (Robertson, 2005; Padman et al., 2009).

Different studies have focused their attention on the inflow of the CDW onto the Ross Sea continental shelf (Budillion et al., 2003; Dinniman et al., 2003; Klinck and Dinniman, 2010; Dinniman et al., 2011; Kohut et al., 2013), but there are no works (using both observational and model data) that we know of that have investigated the seasonal and interannual variability of this inflow.

In this paper we use hydrographic observations and a 10 year time series in the Drygalski Trough (DT) to describe the spatial variability of CDW inflow onto the North West Ross Sea continental shelf and the temporal variability of this intrusion from the daily to the interannual time scales. Furthermore, we investigate the relationship of this variability with the tidal forcing.

2 Data and Methods

2.1 CTD data

Hydrographic profiles were collected during two oceanographic surveys during January 2006 and 2012. The CTD casts were made along two sections shown in Figure 1. Transect A is made only in 2006, while transect B is made for both years (2006 and 2012).

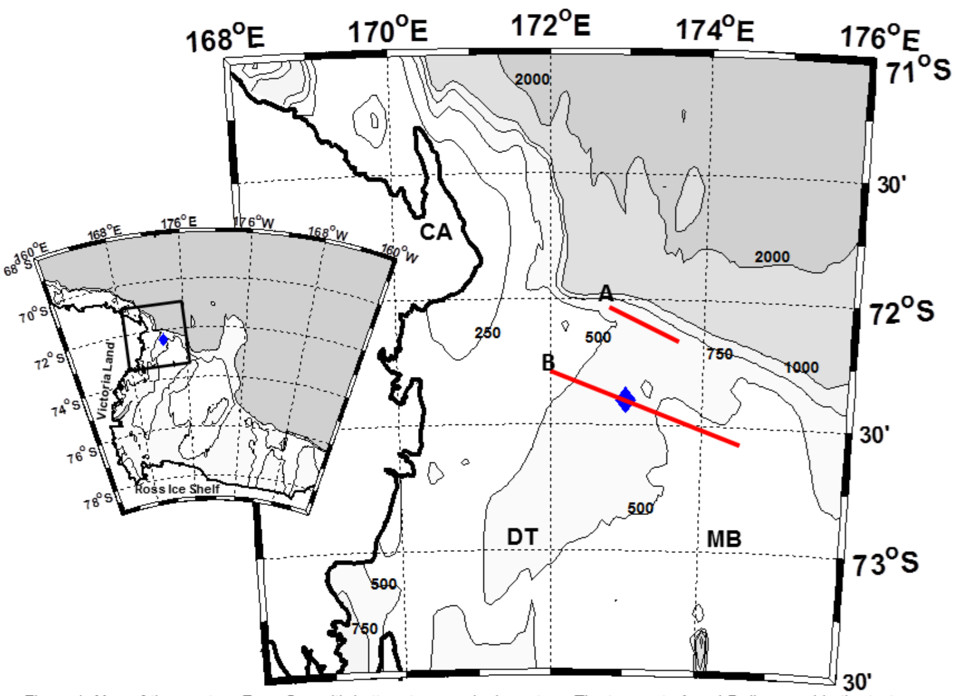

Figure 1: Map of the western Ross Sea with bottom topography in meters. The transects A and B discussed in the text are shown by the red lines. The blue diamond indicates the mooring position. Locations of geographic features discussed in the text are also indicated: Cape Adare (CA), Drygalski Trough (DT) and Mawson Bank (MB).

The CTD data were obtained using a Sea-Bird Electronics SBE 9/11+. The CTD was equipped with dual temperature-conductivity sensors flushed by a pump at constant rate. Calibrations were performed before and after the cruises. Data were acquired at the maximum frequency (24 Hz). The CTD temperature calibration was checked during cruises with SIS RTM4200 digital reversing platinum thermometers. At every station, several samples of water at different depths and salinity ranges were collected and analyzed on board using an Autosal Guideline salinometer. Typical errors were about ±0.003 °C for temperature and 0.005 for salinity. Hydrographic data were corrected and processed according to international procedures (UNESCO, 1988). Standard algorithms (UNESCO, 1983) were used to compute quantities such as θ and S, while γ^n (neutral density) was computed using the Jackett and McDougall (1997) algorithm.

2.2 LADCP data

A Lowered Acoustic Doppler Current Profiler (LADCP) was used during the 2005/06 and 2011/12 cruises. In this paper we show only the results for the transect closest to the shelf break (2005/06 campaign only) in order to emphasize the flow characteristics as close to the shelf break as possible.

The LADCP was composed of two RDI Workhorse 300 kHz ADCP heads mounted on the SBE carousel, one directed upward and the other downward. The two ADCP were set up to work simultaneously, pinging at a maximum rate of about three times per second. To extrapolate the velocity profiles we used the methodology described by Visbeck (2001).

In this paper we decomposed the LADCP current velocity into cross-section (normal to the shelf break – u_x) and along-section (u_a) components.

2.3 Mooring data

A mooring was deployed in the center of the DT at about 50 km from the shelf break between 2004 and 2014 (See Figure 1 for the mooring position). The mooring was equipped with current meters (Aanderaa RCM7), temperature and conductivity sensors (SBE-SeaCat 16 and 39). The mooring had different configurations in different years (Figure 2).

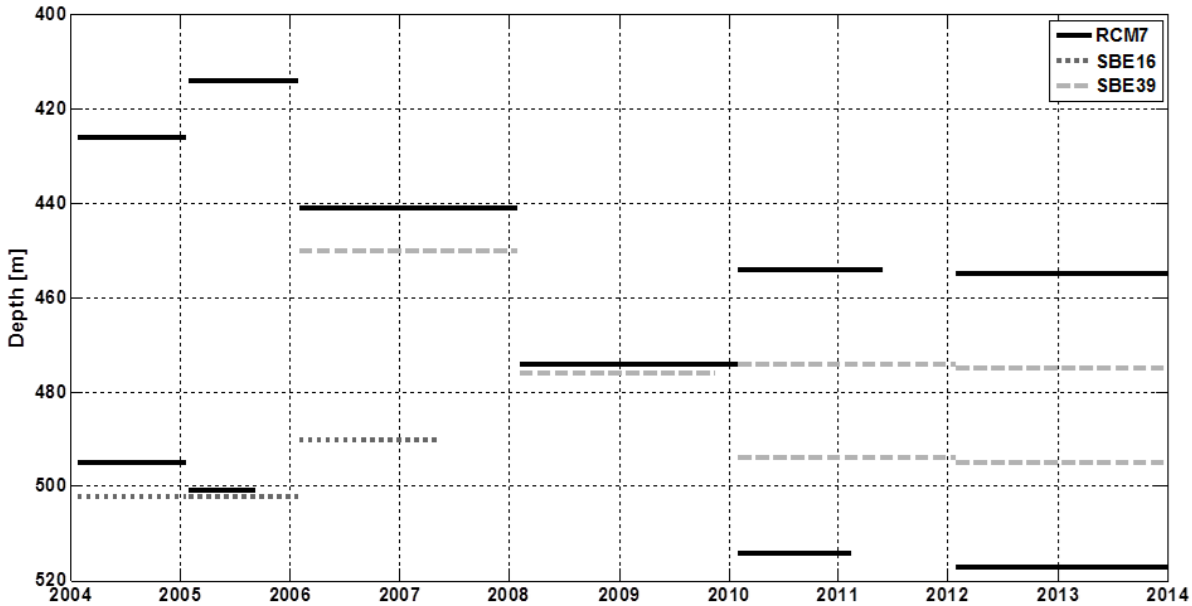

Figure 2: Operation periods for the mooring deployed in the middle of the Drygalski Trough discussed in the text. The different gray lines indicate the instrument type (see legend, upper right).

The accuracy of the individual speed and direction measurements of the Aanderaa RCM7 is ±1 cm s^{-1} and ±5°, respectively. Systematic errors may occur in the RCM7 time series at very low speeds (<1cm s^{-1}); however, measured speeds in the present data set were always well above this threshold level and so we assume errors from this source are negligible. The accuracy of SBE-SeaCat 16 and 39 (temperature only) sensors was checked against CTD casts before and after deployments. See Figure 2 for the operational periods of the different instruments.

2.4 Wavelet analysis

Fourier analysis reveals frequencies present in the whole time series, but does not have any information on aperiodic events (Kantha and Clayson, 2000). Here, we have used the wavelet analysis (Morlet et al. 1982; Morlet 1983; Meyers et al., 1993; Foufoula-Georgiou and Kumar 1995; Burrus et al., 1998; Grinsted et al., 2004; Budillon et al. 2011) to expand the time series into time-frequency space. With this analysis, it is therefore possible to find localized intermittent events (Grinsted et. al., 2004) such as seasonal major intrusions of mCDW.

2.5 Water masses classification

Following Orsi and Wiederwohl (2009), we defined the principal water masses (analyzed in this study) of the Ross Sea using both thermohaline parameters (Salinity S, and potential temperatures θ) and neutral density (γ^n) (Jackett and McDougall, 1997): Antarctic Surface Water (AASW; $\gamma^n < 28.00$ kg m^{-3}, and S < 34.30); Shelf Water (SW; $\gamma^n > 28.27$ kg m^{-3} and θ < -1.85° C); High Salinity Shelf Water (HSSW; ($\gamma^n > 28.27$ kg m^{-3} , θ ≈ -1.85° C and S > 34.62; AABW ($\gamma^n > 28.27$ kg m^{-3} and θ > -1.85° C); CDW ($\gamma^n > 28.00$ kg m^{-3} and θ > 1.2); and mCDW ($28.00 < \gamma^n < 28.27$ kg m^{-3}).

3 Results

3.1. Spatial variability of the mCDW inflow

Two west to east CTD sections across the Drygalski Trough southward of the shelf break (Figure 1) show the characteristics of the CDW inflow over the shelf. At the mouth of the DT, section A (Figure 3) shows the entrance of the CDW already modified from mixing with the Antarctic Slope Current. A relatively warm and less oxygenated layer indicative of mCDW, of about 200 m thickness, lies between the dense HSSW on the bottom and the cold, fresh and well oxygenated AASW. This layer is situated from about 200 m to 400 m depth and is delimitated by the neutral density isopycnals of 28 kg m^{-3} and 28.27 kg m^{-3}, from the dissolved oxygen isoline of 6.2 mgl^{-1} and from the isotherm of 0° C and isohaline of 34.60 from the upper layer. The inflow of CDW is clear from the contours of the current component normal to the shelf break (u_x), where we see a poleward current flux of mCDW and a northward flux of HSSW. Furthermore, through the entire water column the current is moving westward (not shown in Figure) as expected from the geostrophic balance.

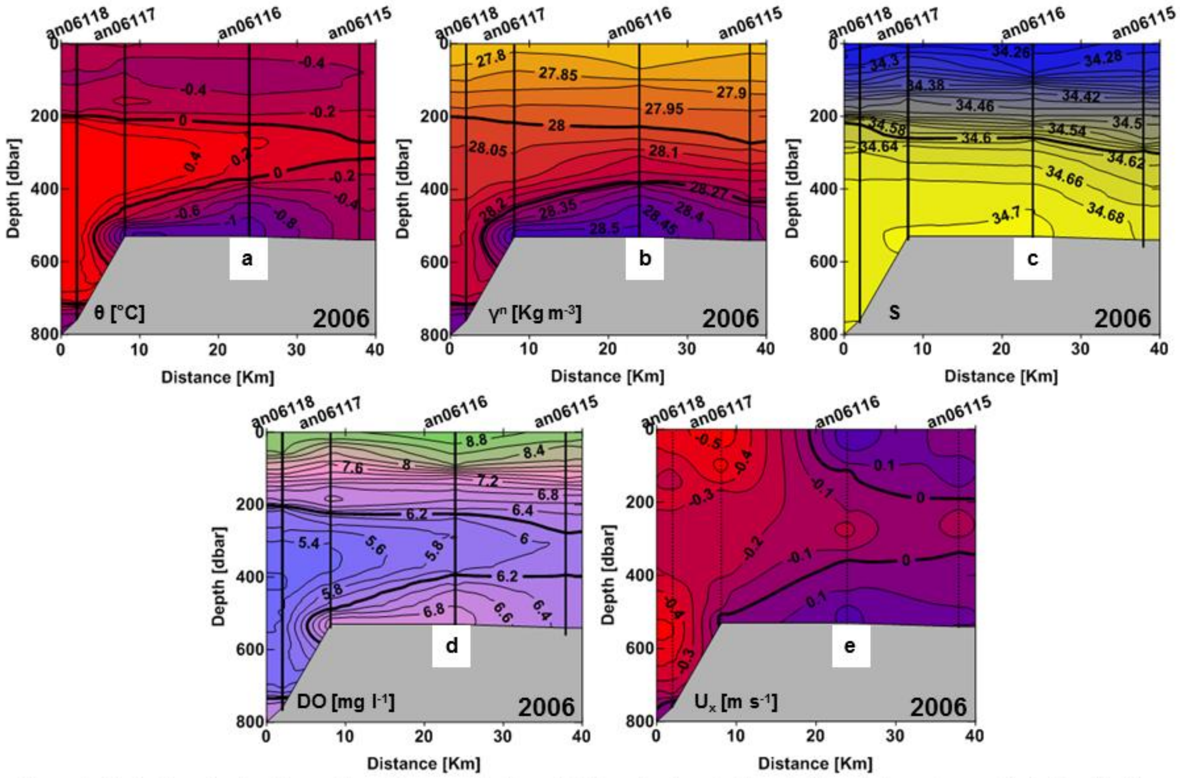

Figure 3: Vertical section looking northward across the Drygalski Trough close to the shelf break (see transect A in Fig. 1): (a) potential temperature θ (°C); (b) neutral density γ^n (kg m^{-3}); (c) salinity S; (d) dissolved oxygen DO (mg l^{-1}); and (e) LADCP velocity (m s^{-1}) for the component normal to the Shelf Break (u_x - positive values directed offshore).

Section B (Figure 4) shows the distribution of the mCDW during two different surveys in 2006 and 2012 at about 50 km from the shelf break (~700 m isobath). For both years, the section identifies the relatively warm potential temperature (greater than -1° C) and neutral density between 28 kg m^{-3} and 28.27 kg m^{-3}. A layer of this relatively warm and less oxygenated water is present across the trough and lies between 200 m and 350 m in the middle of the DT around station #102 in 2006 and #04 in 2012 and from 200 m to the bottom on the east side of the trough (stations #99 in 2006 and #07 in 2012).

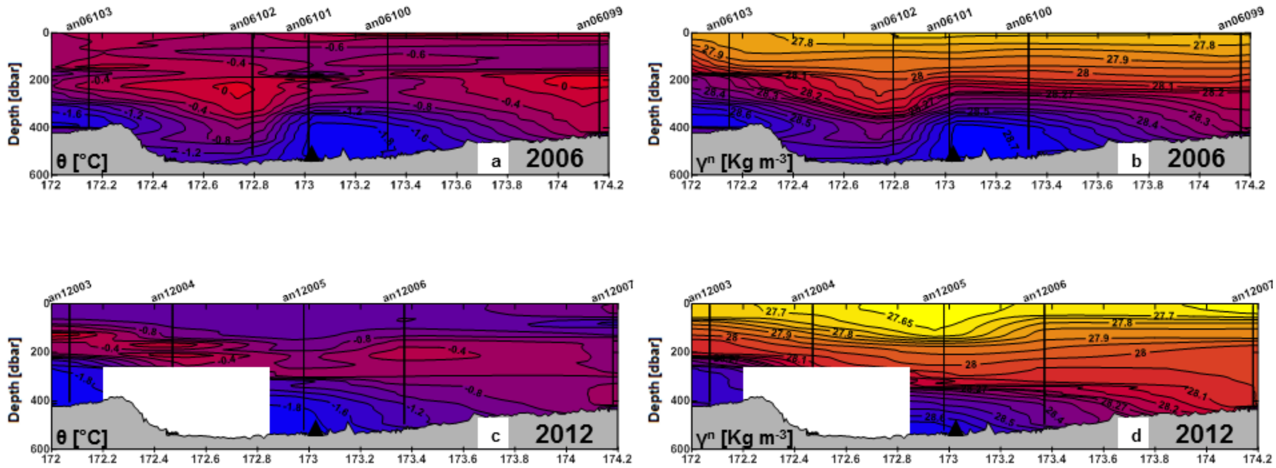

Figure 4: Vertical section across the Drygalski Trough at the mooring location (black triangle), about 50 km from the shelf break (see transect B in Fig. 1) of: (a) potential temperature θ (°C) for the 2006 oceanographic survey; (b) neutral density γ^n (kg m^{-3}) for the 2006 oceanographic survey; (c) potential temperature θ (°C) for the 2012 oceanographic survey; and (d) neutral density γ^n (kg m^{-3}) for the 2012 oceanographic survey.

Previous works using both observational data (Kohut et al. 2013) and numerical models (Wang et al. 2013) suggested that mCDW intrudes onto the shelf mainly on the west slope of the Ross Sea banks. Figure 4 instead highlights the presence of two main cores of MCDW, one on the east side of the trough spreading along the west slope of Mawson bank from about 200 m to the bottom, and another in the central-west side from 200 m to about 350 m.

3.2 Temporal variability of the mCDW inflow

In the CTD section in Figure 4 and in the CTD casts made at the mooring position during different summer cruises (not shown here) a signal of mCDW has never been found at the bottom of DT. However, the salinity and temperature time-series registered by the different sensors on the mooring (Figure 5) from January 2004 to September 2007 periodically show the presence of this relatively warm (T > -1 °C), fresh (S < 34.64) (Figure 5a) and less dense (γ^n < 28.27) water (Figure 5b) in the middle of the trough at about 10 meters above the bottom (mab). The presence of mCDW is also evident in the temperature signal only, up to January 2014 (Figure 6).

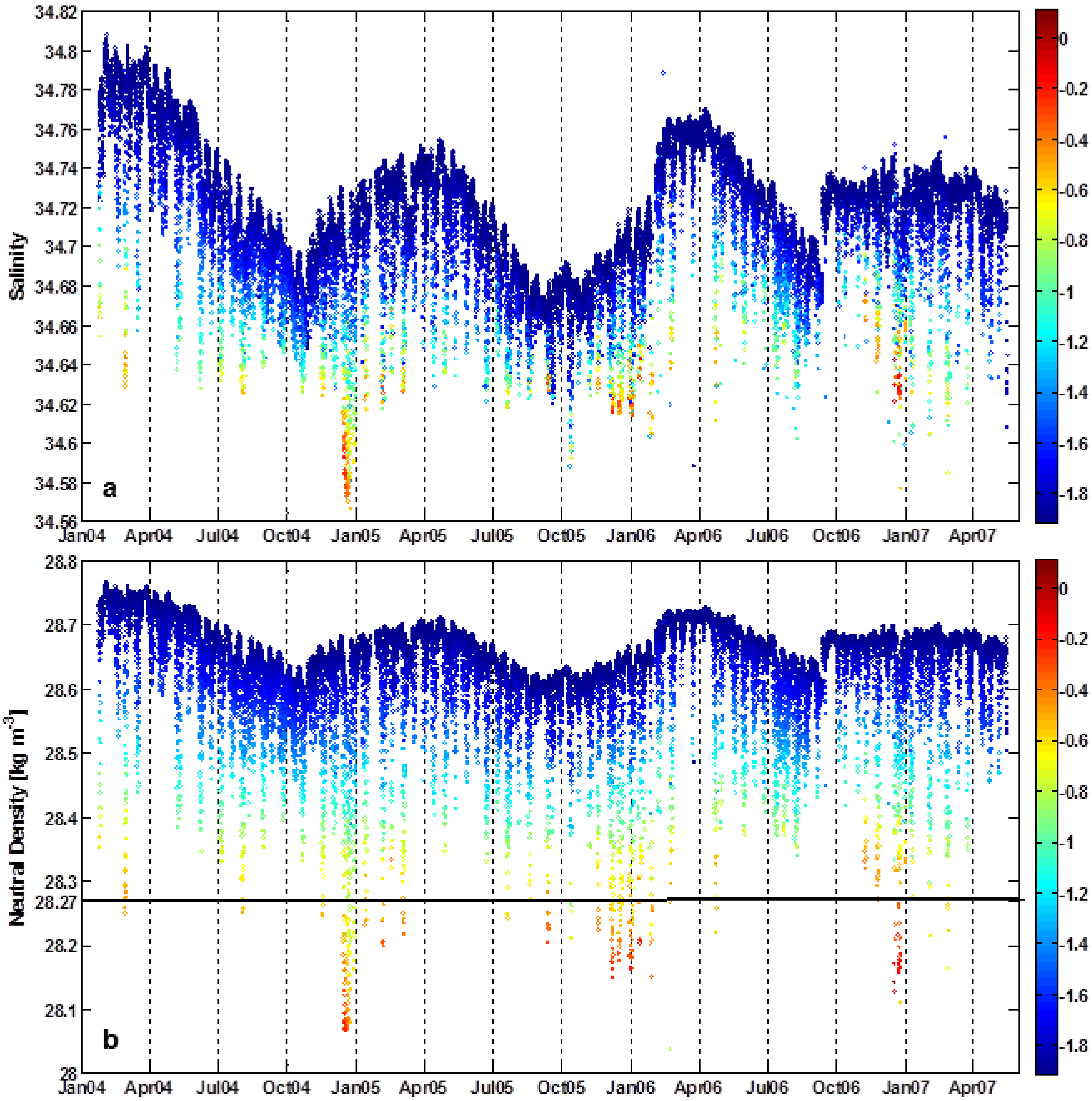

Figure 5: Hourly time series of (a) salinity with temperature (°C) color coded and (b) neutral density γ^n (kg m^{-3}) with temperature (°C) color coded, registered by the bottom instruments on the mooring in the middle of the Drygalski Trough (see Fig. 1 for location).

In Figure 6 we always used the data registered by the bottom sensors (Figure 2), except for the 2006-2008 time series, where we used the upper sensor (black scatter in Figure 6), because the bottom sensor stopped working in May 2007. This does not change our results.

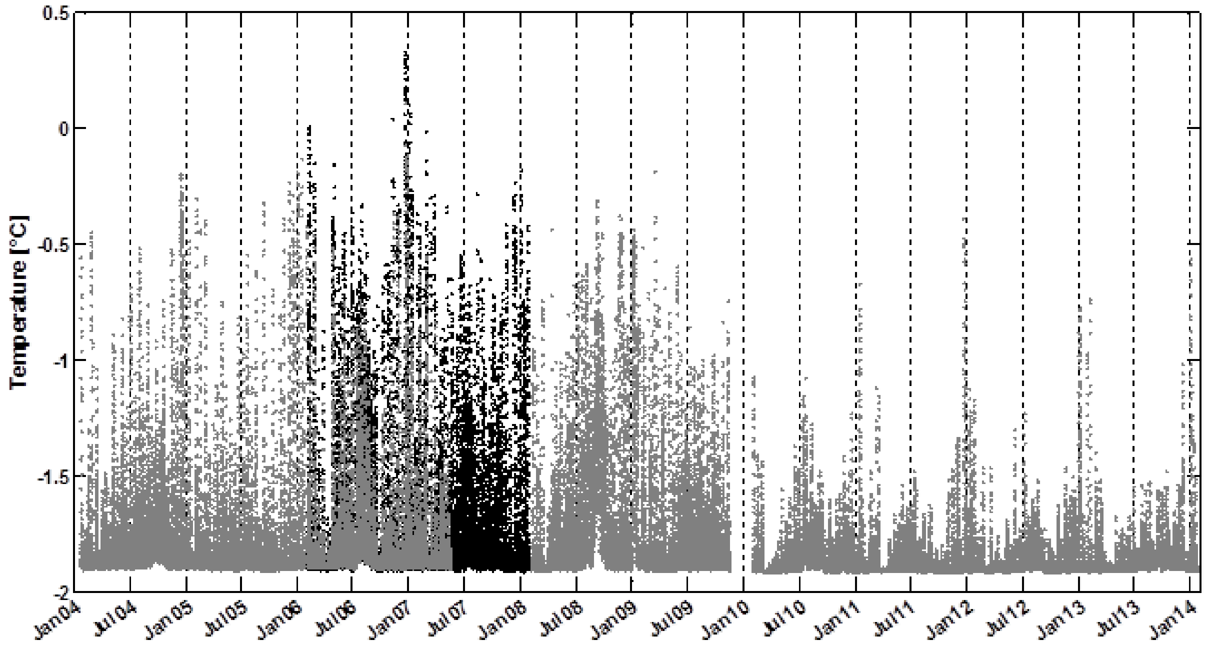

Figure 6: Hourly time series of the temperature (°C), registered by the bottom instruments (about 20 m above the bottom; in grey) and by the upper instrument (about 80 m above the bottom; in black) on the mooring in the middle of the Drygalski Trough (see Fig. 1 for location).

In the time series plots (Figures 5 and 6), it is shown that these intrusions of mCDW into the bottom layer have a daily and a fortnightly variability (about 13.66 days), which in earlier works have been attributed, respectively, to the influence of the daily and spring/neap tidal cycles (Whitworth and Orsi, 2006; Padman et al., 2009). This periodicity is also evident in the wavelet power spectrum of the 2 year time series from January 2012 (Figure 7). In particular, the daily frequency is present in all the different parameters throughout the entire time series (with some exceptions that will be stressed later), while the fortnightly frequency is more evident in the wavelet power spectrum of the intensity of the current and in the temperature signal and less evident (but still present) in the meridional and zonal velocity components.

A strong seasonal variability of mCDW intrusions is also clear from Figures 5 and 6. It appears that a strong incursion of mCDW occurs each austral summer around the end of December/beginning of January. In addition, a relatively high presence of mCDW is often registered by the bottom instruments around July.

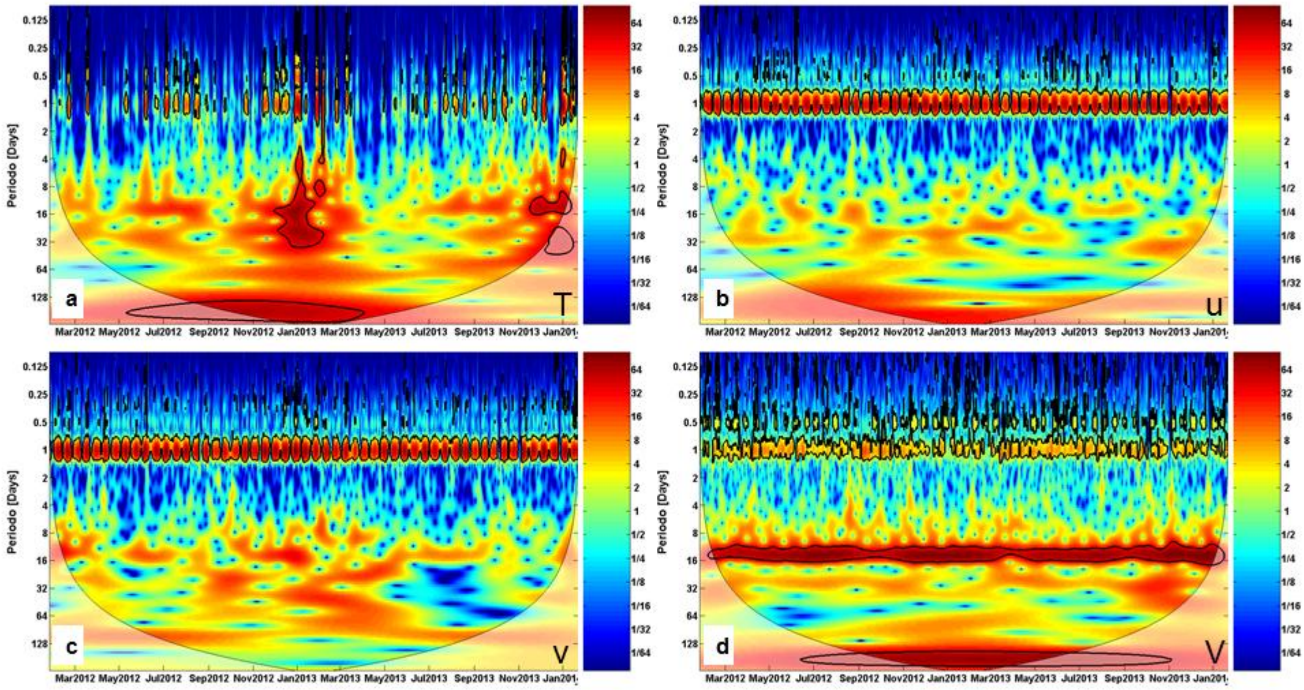

Figure 7: Wavelet power spectrum for the 2012 - 2014 time series registered by the bottom sensors (about 20 m above the bottom), on the mooring in Fig. 1, of the (a) temperature (°C) (T); (b) zonal component (u, ms^{-1}) of the bottom current; (c) meridional component (u, ms^{-1}) of the bottom current; and (d) magnitude (V, ms^{-1}) of the bottom current meter. The significance level (thick black line, 95%) and the cone of influence (thin black line) are also indicated.

This seasonal intrusion is further emphasized in Figure 5b, where the density of the water reaches values lower than 28.27 in neutral density, the threshold indicative of mCDW (Orsi and Wiederwohl, 2009). Moreover, it is important to note that almost no presence of mCDW is found around March/April in correspondence to the salinity maximum (and the temperature close to the surface freezing point) associated with the HSSW.

The maximum mCDW inflow is observed in December/January, a few months after the salinity minimum registered around October that indicates the lowest presence of HSSW (Figure 5a). This may suggest that these weaker intrusions of less dense water to the bottom of the trough are not related to the thicker layer of the denser shelf water (HSSW) that can act as a limitation to the vertical mixing.

The wavelet power spectrum (Figure 7) of the temperature (Figure 7a) shows this isolated signal (stronger inflow of mCDW) with a strong energy in the power spectrum around January 2013 and 2014 from the low frequency (period of 32 days) to the high frequency (period of few hours). This strong energy does not exist either in the velocity current components (Figure 7b,c), nor in the current intensity (Figure 7d) signals. Another large difference shown by the wavelet analysis is the lack of energy in the temperature power spectrum in both the diurnal and fortnightly tidal harmonics around March-April that corresponds to the time of the salinity maximum. The energy does not disappear at this time in the wavelet power spectrum of the current.

These characteristics of the wavelet power spectrum are similar to all the wavelet power spectra (not shown here) made for the different time-series registered by the instruments through the entire sampling period from 2004 to 2014.

In addition to a seasonal signal, interannual variability is also clear. In Figure 6 there is a change in the temperature signal daily fluctuations before and after 2010. Strong daily fluctuations are present through the entire time-series from 2004 to 2010, while they are much less evident from 2010 to the end of the time series.

Despite our analysis depending on a bottom instrument that changes its depth over the life time of the mooring series, we believe that this does not affect the results. Neither the seasonal nor the interannual variability depends on the depth of the sensors.

In Figure 6, it is clear that both time series measured at 20 mab (grey) and 80 mab (black), in 2006, have the same seasonality with minimum values in March-April and maximum in January. Moreover, both time series have similar oscillations at both depths, which are much stronger than the oscillations recorded after 2010. Thus, large differences in the temperature oscillation before and after 2010 do not depend on the distance from the bottom.

In addition, despite the distance of the instrument from the bottom in 2004 and 2015 being almost the same (respectively 12 mab and 15 mab), there is a large difference in the temperature oscillation. In 2010 the sensor is 28 m from the bottom and the temperature has much less oscillation compared to 2004 (12 mab) and 2005 (8 mab).

Fourier analysis of all the time series over the whole sampling period at all depths (not shown here) for temperature, zonal and meridional current components, and for the current magnitude shows that the most energetic contributions to the tide are the diurnal tidal harmonics K_1 (period 23.92 h) and O_1 (period 25.84 h). This is followed by P_1 (period 24.04 h) and Q_1 (period 26.88 h), and from the lunar fortnightly constituent MF (13.66 days). The same results are obtained using the T_tide Matlab routines (Pawlowicz et al., 2002), which are based on the methods described by Foreman (1978). Table1 reports the characteristics of the major tidal constituents together with the M_2 for each current meter.

Deployment Year	Instrument Depth (m)	Tide	Freq (cph)	Umaj (ms^{-1})	Umin (ms^{-1})	Inc (°N)	Pha (°)
2004	426	MF	0.0031	0.048	-0.008	236.72	76.51
		Q1	0.0372	0.058	0.041	210.58	128.85
		O1	0.0387	0.301	0.208	208.72	135.03
		P1	0.0416	0.100	0.070	198.17	169.25
		K1	0.0418	0.303	0.217	195.58	168.32
		M2	0.0805	0.022	0.008	202.23	44.82
2004	495	MF	0.0031	0.026	0.001	193.23	86.15
		Q1	0.0372	0.042	0.029	192.25	114.64
		O1	0.0387	0.232	0.160	193.03	122.74
		P1	0.0416	0.075	0.050	175.27	147.98
		K1	0.0418	0.233	0.162	174.45	148.70
		M2	0.0805	0.045	0.024	147.75	73.28
2005	414	MF	0.0031	0.061	-0.007	241.55	63.35
		Q1	0.0372	0.060	0.036	206.26	86.82
		O1	0.0387	0.320	0.212	213.41	107.21
		P1	0.0416	0.104	0.075	194.23	129.17
		K1	0.0418	0.294	0.213	200.5	135.37
		M2	0.0805	0.052	0.044	192.14	10.03
2005	501	MF	0.0031	0.021	-0.005	236.26	99.00
		Q1	0.0372	0.045	0.030	202.71	99.91
		O1	0.0387	0.246	0.178	207.49	112.56
		P1	0.0416	0.083	0.055	170.66	116.22
		K1	0.0418	0.236	0.185	186.14	131.89
		M2	0.0805	0.053	0.044	157.15	25.27
2006	441	MF	0.0031	0.051	-0.011	248.06	176.36
		Q1	0.0372	0.068	0.039	217.72	269.21
		O1	0.0387	0.324	0.208	217.39	194.43
		P1	0.0416	0.104	0.071	206.06	334.64
		K1	0.0418	0.310	0.211	205.56	334.57
		M2	0.0805	0.047	0.039	190.84	299.92
2008	474	MF	0.0031	0.038	-0.003	220.38	73.37
		Q1	0.0372	0.056	0.033	207.88	190.07
		O1	0.0387	0.289	0.192	206.72	196.97
		P1	0.0416	0.110	0.071	196.23	233.56
		K1	0.0418	0.295	0.195	194.19	235.58
		M2	0.0805	0.038	0.021	160.31	235.80
2010	454	MF	0.0031	0.045	-0.008	167.95	232.85
		Q1	0.0372	0.055	0.032	144.87	152.42
		O1	0.0387	0.306	0.200	142.52	171.00
		P1	0.0416	0.101	0.071	133.01	219.91
		K1	0.0418	0.304	0.213	131.11	221.72
		M2	0.0805	0.025	0.020	113.67	352.02
2010	514	MF	0.0031	0.034	0.000	148.56	221.18
		Q1	0.0372	0.039	0.021	134.14	12.63
		O1	0.0387	0.230	0.134	135.16	25.17
		P1	0.0416	0.075	0.053	128.89	63.90
		K1	0.0418	0.225	0.153	123.16	62.15
		M2	0.0805	0.021	0.017	234.23	215.14
2012	455	MF	0.0031	0.034	-0.008	190.47	269.55
		Q1	0.0372	0.052	0.032	143.35	285.00
		O1	0.0387	0.284	0.190	140.79	148.24
		P1	0.0416	0.106	0.075	130.8	112.38
		K1	0.0418	0.290	0.212	126.68	232.34
		M2	0.0805	0.026	0.020	123.46	335.22
2012	517	MF	0.0031	0.033	-0.003	160.3	227.36
		Q1	0.0372	0.046	0.021	136.9	311.87
		O1	0.0387	0.256	0.135	136.3	327.66
		P1	0.0416	0.087	0.050	130.94	7.46
		K1	0.0418	0.250	0.151	126.77	4.58
		M2	0.0805	0.033	0.018	119.72	24.33

Table 1: tidal Parameters, computed using T_tide, for the single instruments for each survey: tide constituent frequency (Freq, cycles/hour), major and minor axis (U_{maj} U_{min}, cm s^{-1}), tidal ellipse inclination (Inc, °N) and phase to the Greenwich meridian(pha, °)

4 Discussion

4.1. Tidal mixing

In section 3, it has been shown that a CDW layer of about 200 m enters the mouth of the DT at mid-depth around 300 m (Figure 3). It is thought that CDW intrudes onto the Ross Sea continental shelf in areas where the bottom topography changes direction relative to the slope flow (Klinck and Dinniman, 2010). Then, helped by tidal advection, it is moved across the sill (Whitworth and Orsi 2006, Padman et al., 2009) and transported by a barotropic flow southward (Kohut et al., 2013) where it reaches the mooring location at about the same depth found at the mouth of the DT (Figure 4).

mCDW detected at the bottom of the mooring reaches salinity as low as 34.56 and temperature higher than -0.5°C (Figure 5a). These values show that occasionally the bottom layer is filled with mCDW only. From the θ/S diagrams (Figure 8) of the bottom instrument time series, from January 2004 to February 2007, it is clear there is a presence of only two source water masses: mCDW (temperature close to -0.5°C and salinity lower than 34.65) and HSSW (temperature close to the surface freezing point and salinity that varies between 34.65 and 34.8 depending on the season: saltier at the end of the summer-early fall and fresher toward the austral spring).

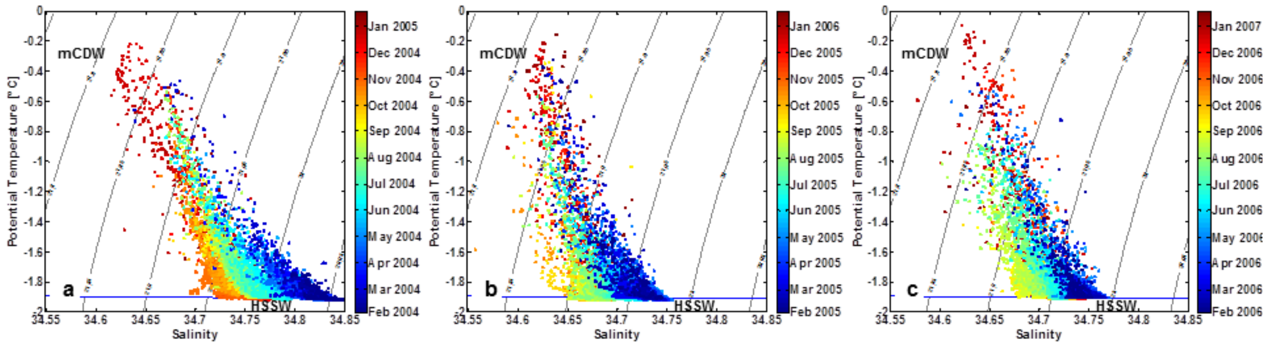

Figure 8: Potential temperature/salinity (θ/S) scatter plot of the (a) 2004 – 2005 time series; (b) 2005 – 2006 time series and (c) 2006 – 2007 time series. The blue horizontal line shows the surface freezing point of seawater.

A product of the mixing of these two source water masses is shown by the spread of the dots along the (imaginary) mixing line between mCDW and HSSW. This is clear throughout all seasons.

The mechanism that brings mCDW from mid-depth to the bottom and increases the relative mixing with the HSSW, is most probably related to the tidal stirring as shown by Whitworth and Orsi (2006). They used mooring data at about 17 km from the shelf break inside the narrow area close to the shelf break influenced by the strong tides that move the ASF up to 20 km from the 700 m isobaths (Padman et al., 2009). Our mooring, instead, is located 33 km south of their mooring and is located always south of the ASF. Nevertheless, in Figure 9 the role of the tide on the intrusion of the mCDW into the bottom layer is evident.

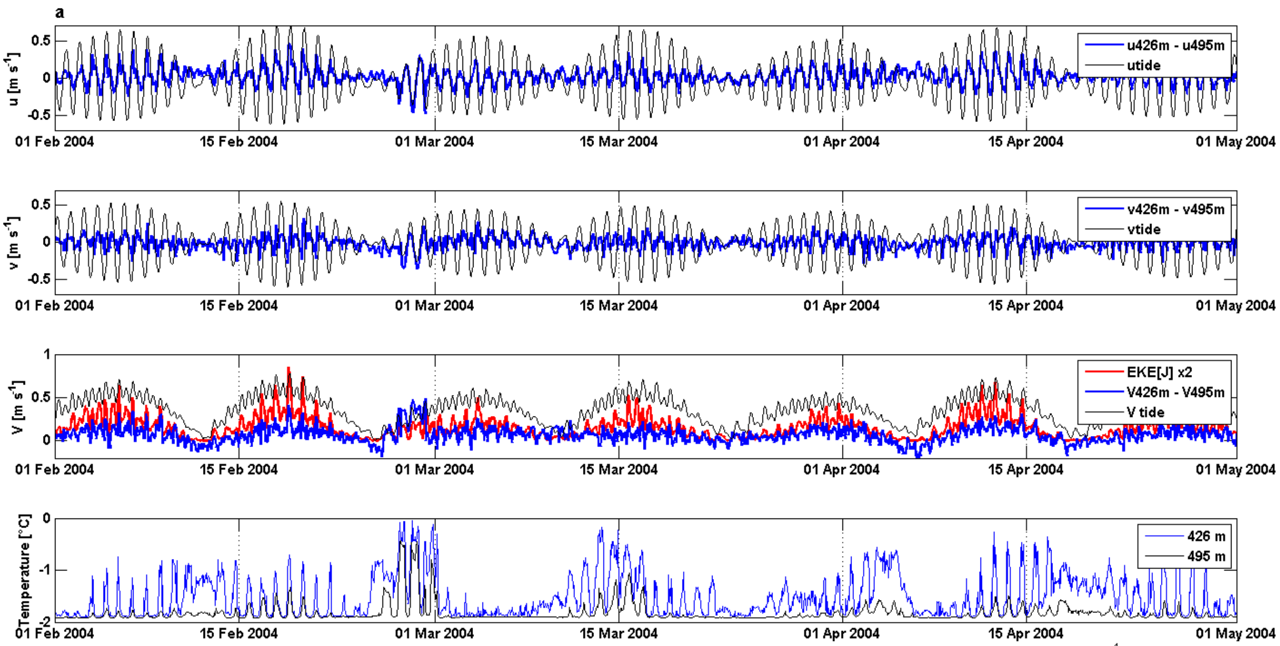

Figure 9: three-months subsets from (a) February; (b) November 2004; (c) February 2013; (d) November 2013; of (starting from the top): (first panel) the zonal component (u, m s^{-1}) differences between the upper and the bottom sensors (thick blue line), tidal component of u (thin black line); (second panel) meridional component (v, m s^{-1}) differences between the upper and the bottom sensors (thick blue line), tidal component of v (thin black line); (third panel) current velocity (V, m s^{-1}) differences between the upper and the bottom sensors (thick blue line), tidal component of V (thin black line), Eddy Kinetic Energy (EKE, J – thick red line) for the bottom sensors scaled for 2; (fourth panel) temperature (°C) registered by the bottom (thin black line) and upper (thin blue line) sensors.

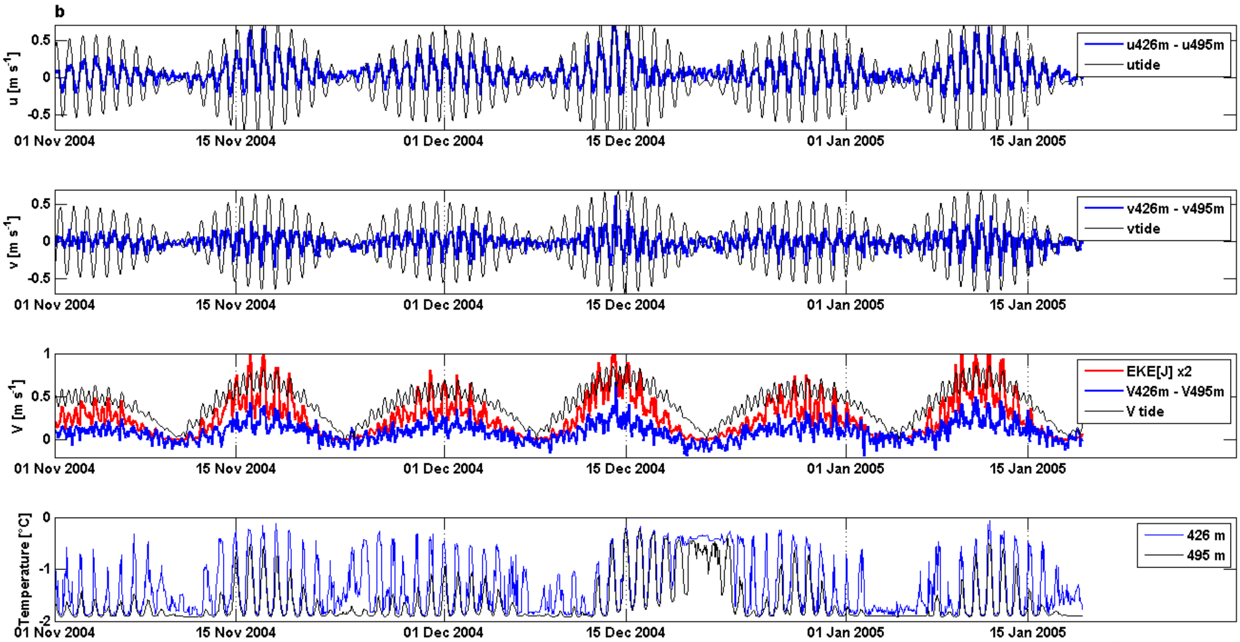

Figure 9: three-months subsets from (a) February; (b) November 2004; (c) February 2013; (d) November 2013; of (starting from the top): (first panel) the zonal component (u, m s^{-1}) differences between the upper and the bottom sensors (thick blue line), tidal component of u (thin black line); (second panel) meridional component (v, m s^{-1}) differences between the upper and the bottom sensors (thick blue line), tidal component of v (thin black line); (third panel) current velocity (V, m s^{-1}) differences between the upper and the bottom sensors (thick blue line), tidal component of V (thin black line), Eddy Kinetic Energy (EKE, J – thick red line) for the bottom sensors scaled for 2; (fourth panel) temperature (°C) registered by the bottom (thin black line) and upper (thin blue line) sensors.

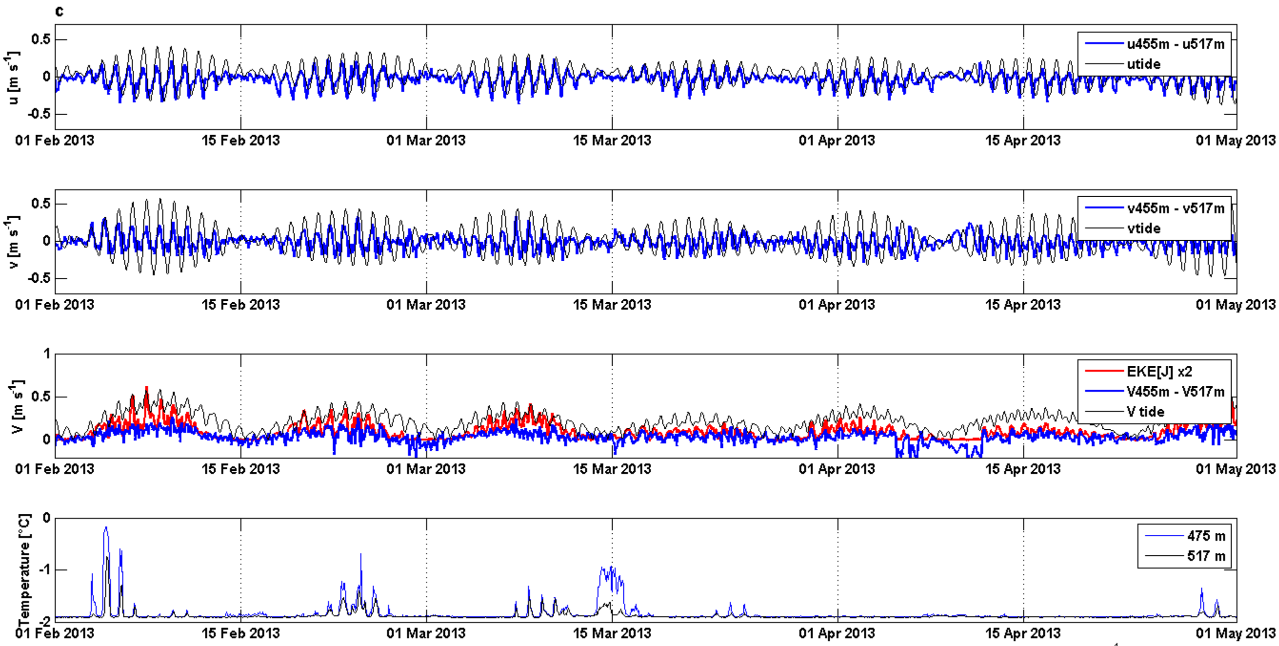

Figure 9: three-months subsets from (a) February; (b) November 2004; (c) February 2013; (d) November 2013; of (starting from the top): (first panel) the zonal component (u, m s^{-1}) differences between the upper and the bottom sensors (thick blue line), tidal component of u (thin black line); (second panel) meridional component (v, m s^{-1}) differences between the upper and the bottom sensors (thick blue line), tidal component of v (thin black line); (third panel) current velocity (V, m s^{-1}) differences between the upper and the bottom sensors (thick blue line), tidal component of V (thin black line), Eddy Kinetic Energy (EKE, J – thick red line) for the bottom sensors scaled for 2; (fourth panel) temperature (°C) registered by the bottom (thin black line) and upper (thin blue line) sensors.

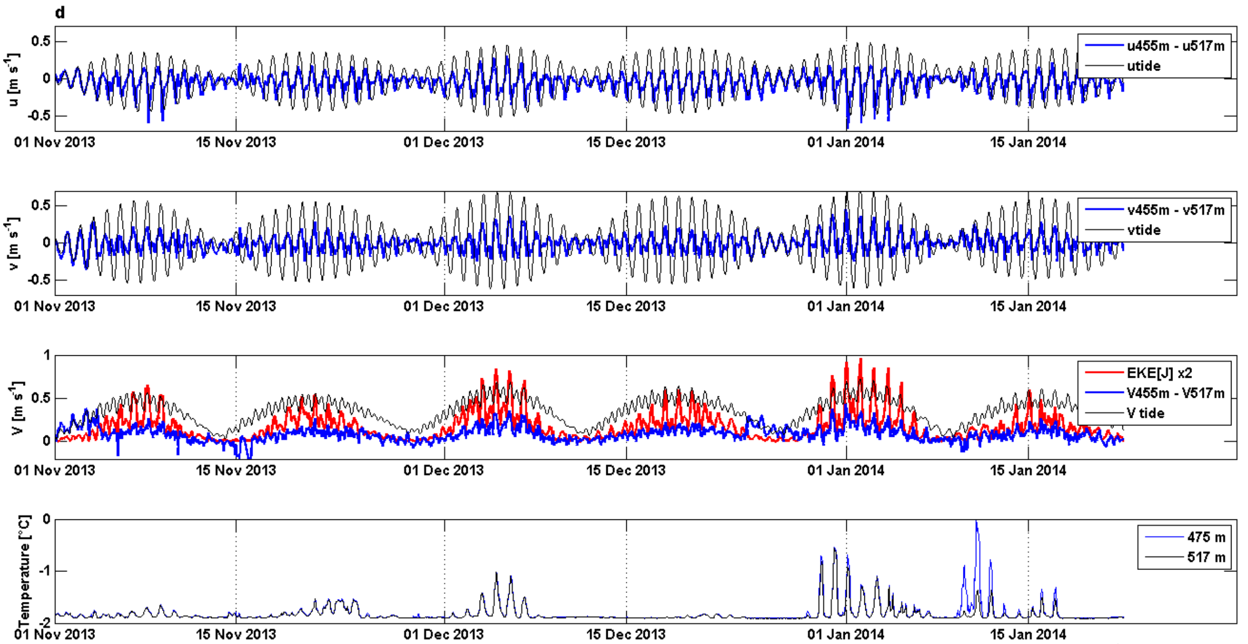

Figure 9: three-months subsets from (a) February; (b) November 2004; (c) February 2013; (d) November 2013; of (starting from the top): (first panel) the zonal component (u, m s^{-1}) differences betwee the upper and the bottom sensors (thick blue line), tidal component of u (thin black line); (second panel) meridional component (v, m s^{-1}) differences between the upper and the bottom sensors (thick blu line), tidal component of v (thin black line); (third panel) current velocity (V, m s^{-1}) differences between the upper and the bottom sensors (thick blue line), tidal component of V (thin black line), Eddy Kine Energy (EKE, J – thick red line) for the bottom sensors scaled for 2; (fourth panel) temperature (°C) registered by the bottom (thin black line) and upper (thin blue line) sensors.

In particular, this is clear when comparing the velocity current differences (zonal and meridional components and the magnitude of the current) between the bottom (19 mab in 2004 and 15 mab in 2013) and the upper sensors (88 mab in 2004 and 77 mab in 2013), and examining the Eddy Kinetic Energy (EKE) and the tidal kinetic Energy (KE) of the bottom sensors (Figure 9). In the figure, it is evident that during strong tidal flow the velocity differences between the two levels usually increase, with a maximum shear during spring tides. At the same time there is an increase of the EKE at the bottom instrument and a related high temperature signal registered at both levels.

In addition, it is evident that the temperature increase is detected first at the top instrument then at the bottom sensor. This could be evidence that the warming signal comes from the top layer.

The hypothesis that the water measured at the bottom layer by the sensors on the mooring is a result of the lateral flux coming from the Mawson Bank is rejected, firstly, because we do not see any correlation (relationship) of the temperature with the zonal component of the current and secondly, when the tidal ellipse of the main tidal constituents is perpendicular to the DT and whence we could expect a major westward flow, the temperature fluctuation registered is actually lower.

Indeed, we can hypothesize that the tide induces a vertical shear that increases the Eddy Kinetic Energy and therefore triggers the mixing of the bottom 200-300 m at least, bringing the mCDW to the bottom. It has been suggested in a modeling study of the area (Padman et al., 2009) that diapycnal diffusivity can be substantially increased through the lower 300 m of the water column, at least over the sill, during a portion of each diurnal tidal cycle at spring tide. Thus, thanks to the tidal stirring, the mCDW arrives at the bottom of the DT 50 km south of the shelf break (about 33 km south of where it was detected by Whitworth and Orsi 2006), changing the characteristics of the bottom layer and being an efficient mechanism, as was hypothesized by Foster et al. (1987), to produce a water mass with characteristics intermediate between HSSW and mCDW (the Antarctic Bottom Water) and to influence the shelf water outflow.

4.2. mCDW inflow at different time scales

4.2.1 seasonal variability

From the mooring data analyzed in the previous section, we observed a six month seasonal variability with two peaks of mCDW registered in the benthic layer. A stronger presence is found around December-January and a weaker one around July. In the prior paragraph we have shown a strict relationship between the tide and temperature signal on the small temporal scale. Here we hypothesize that the tide has a role on longer time scales too. In Figure 10 we compare the EKE, the tide KE and the temperature signals low-pass filtered with a cutoff of 15 days over the entire sampling period. In this case the strong relationship between those signals is evident, with the three time series covarying with six-month seasonal variability. High EKE, tide KE and warm temperature are shown in January and July with minimum values in March and October. This confirms that the mCDW inflow seasonal variability may be only tide related.

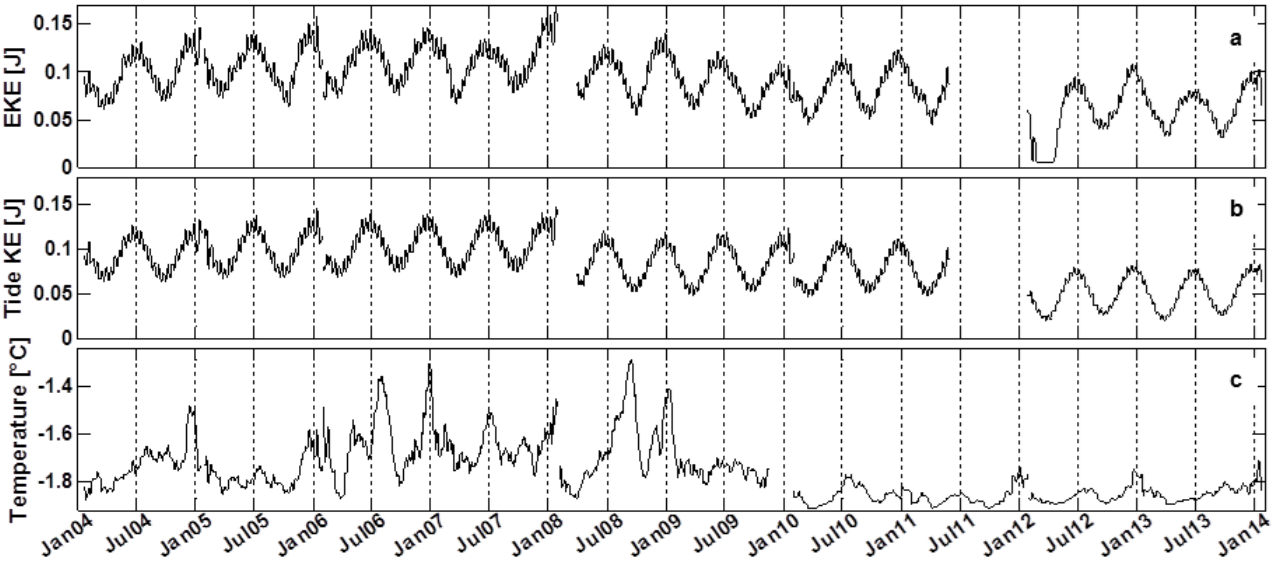

Figure 10: low-pass filtered (with a cutoff of 15 days) time series of the (a) Eddy Kinetic Energy (EKE, J); (b) tidal kinetic Energy (Tide KE, J) and (c) temperature (°C) registered by the bottom sensors over the entire sampling period from January 2004 to January 2014.

However, we also consider other hypotheses. Firstly, following Klinck and Dinniman (2010), the CDW onshore flux over the Ross Sea depends on the inertia of the flow in the presence of bathymetry that curves offshore in front of along-slope flow. Therefore, we postulated that an intensification of the Ross Gyre would strengthen the along-slope westward current (southern limb of the gyre) and therefore favor momentum advection over the shelf.

Using the ECMWF (European Centre for Medium-Range Weather Forecasts) ERA-interim reanalysis (Dee et al., 2011), we looked for any seasonality of the wind curl over the Ross Gyre (that can be an indication of the intensification of the gyre) and for some correlation of this signal with the temperature registered by the mooring (not shown here), but we did not find any, so we disregard this hypothesis.

Secondly, looking at the wind component parallel to the shelf break at the DT from 2004 to 2011 (Figure 11, negative values towards north-west) and comparing it to the mCDW intrusions, we find the lowest presence of mCDW at the bottom of the mooring (Figure 10) during stronger easterlies in February-March and the maximum mCDW intrusions during weak westward winds in December-January. These results are in accordance with Stewart and Thompson (2015), who in their model saw that increasing the easterly wind stress over the slope steepens the isopycnal in the ASF, deepening the pycnocline at the shelf break until CDW can no longer mix across it. Thus we can speculate that during strong easterlies we may have a weak advection of CDW over the shelf and the contrary during feeble westward winds.

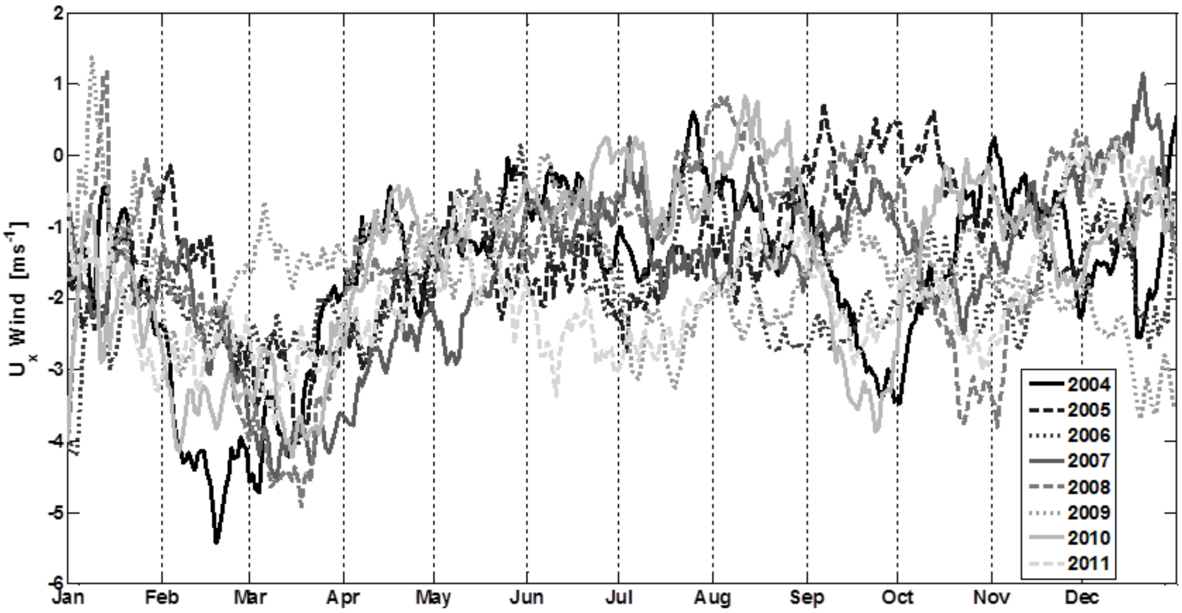

Figure 11: Monthly average along shelf break wind component from 2004 to 2011 (see legend lower right for the different years) of the daily mean ERA-interim (ECMWF) time series. The data where averaged over the area close to the shelf break in the western Ross Sea (from 71.5° S to 72.5° S & from 172° E to 176° E). The along-shelf break wind component is obtained rotating the coordinate system by 26° so that one component roughly aligns with the Ross Sea shelf break line in the subset area.

Furthermore, the deepening of the pycnocline may favor the escape of dense water from the shelf, pulling the HSSW toward the northern limit of the continental shelf and consequently filling the bottom layer in March - April with a thick layer of HSSW (Budillon et al. 2011). This may prevent mCDW from arriving at the bottom of mooring G during spring tide because there is not enough kinetic energy deriving from tidal dissipation that has the strength to overcome the vertically-averaged potential energy from stronger stratification caused by the thicker HSSW layer.

Indeed, here we speculate that the seasonal intrusion of mCDW into the bottom layer is governed by the tides, but may be modulated by the wind fields.

4.2.2 Interannual variability

Besides a seasonal variability, the results in section 3.2 (Figure 6) show a large difference in the temperature oscillation before and after 2010.

Examining the ellipse inclinations of the main tidal constituents O_1 and K_1 (Table 1 and Figure 12) it is evident that there is a change of the orientation from (almost) parallel to the major axis of the Drygalski Trough (before 2010) to perpendicular to it (after 2010). The same occurs for the other main tidal harmonics reported in table 1 (P_1 Q_1 MF).

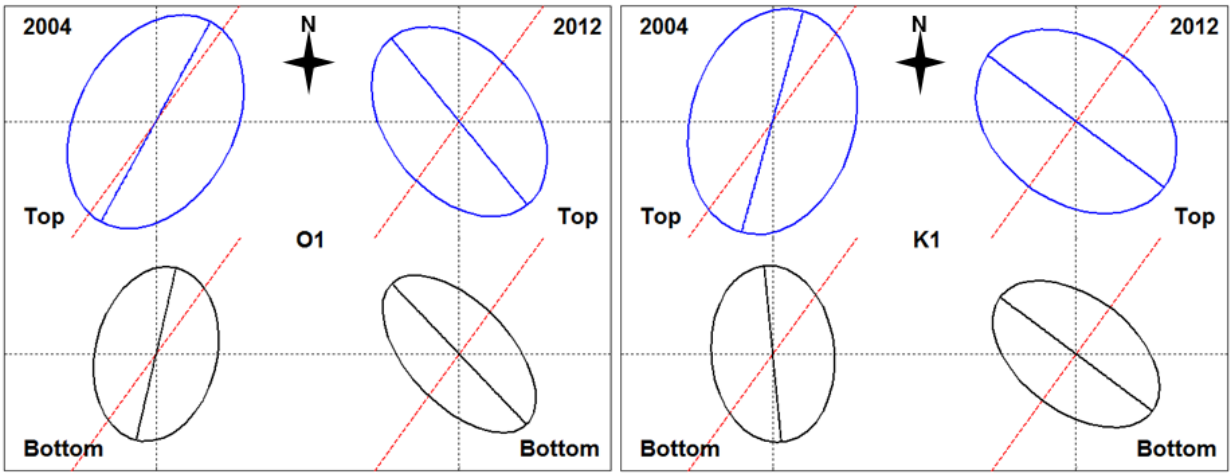

Figure 12: Tidal ellipses of the main constituents O_1 (left panel) and K_1 (right panel) at different depths throughout the entire sampling period for the 2004 (left) and 2012 (right) mooring time series. The red lines indicates the direction of the Drygalski Trough main axis (about 36° N).

We believe that this shift in the ellipses orientation plays a role in the change of the temperature signal fluctuation. Prior to 2010 the tide has a stronger along trough component, i.e. a stronger cross slope component, thus the onshore transport of mCDW toward the mooring increases.

Besides the ellipse orientation shift, after 2010, the bottom tide KE and EKE (Figure 10), together with the current shear between the two layers (Figure 9) decreases drastically.

Probably this modification of the tidal ellipses and of the tide behavior in general is caused by a change in the stratification before and after 2010. According to Muller (2012), different factors may modify the tide behavior, including changes in the stratification. In addition, Pereira et al. (2002) observed that there is seasonality in the mixing induced by tides as a result of the change in the stratification.

A change in the stratification is actually detected in the CTD data and in the mooring time series. Looking at the θ/S diagram (Figure 13) of the transect B (Figure 4), a more homogenous bottom layer in 2012 is evident. In fact, the θ/S profiles between mCDW and HSSW (Figure 13b) in 2012 are almost parallel to the isopycnals, while in 2006 the θ/S profiles (Figure 13a) are more perpendicular to them, showing a more stratified benthic layer.

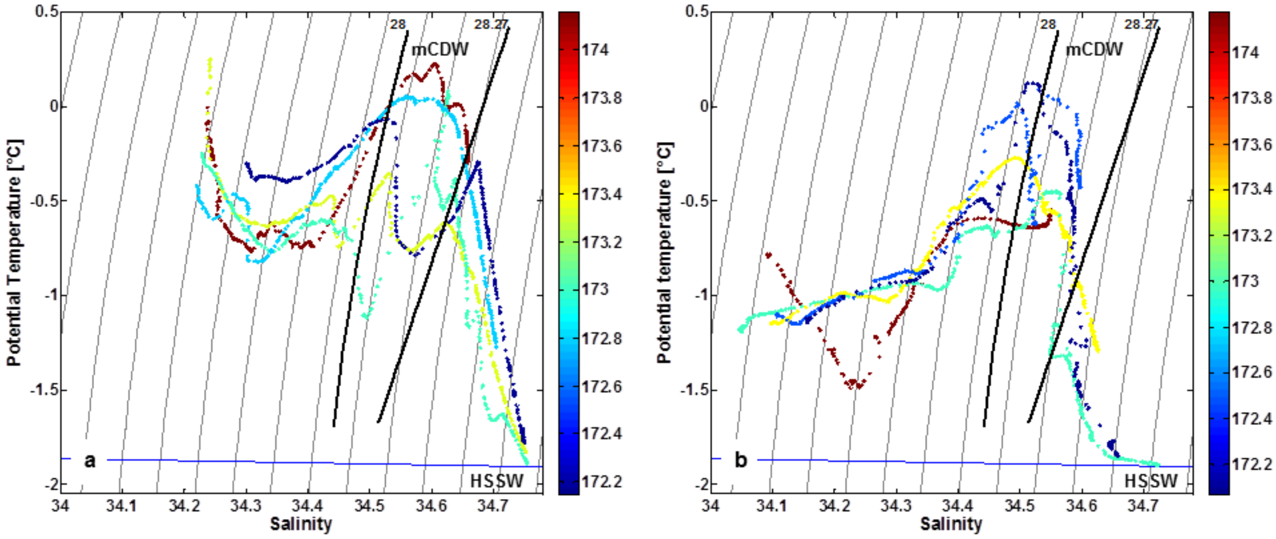

Figure 13: Potential temperature/salinity (θ/S) scatter plot of the transect B (see Figures 1 and 4), color coded by the longitude (°E), for the (a) 2006 oceanographic survey and (b) 2012 oceanographic survey. The blue horizontal line shows the surface freezing point of seawater.

The temperature time series (Figure 9) also shows a different behavior from 2004 to 2013. In 2004 (Figures 9a and 9b, bottom slice), the temperature measured by the upper sensor almost always diverges from the temperature registered by the lower sensor (the divergence increases during the spring tides). While in 2013 (Figures 9c and 9d, bottom slice), the temperature discrepancy is always close to zero except during spring tide events, indicating a more homogenous bottom layer in the 2010-2014 time series.

Moreover, an evidence of a shift in the benthic layer stratification towards a more homogenous structure is also obvious when comparing the tidal ellipses at different depths throughout the entire sampling period. Before 2010 the bottom tidal ellipses for all the main tidal constituents are oriented to the west of the upper layer ellipses (Table 1 and Figure 12). However, after 2010 the bottom and top ellipses have almost the same orientation. For example, in Figure 12 it is clear that in 2004 the bottom tidal ellipse is oriented to the west of the one in the upper layer by 15.69° for O_1 and 21.13° for K_1, while in 2012 the bottom and top ellipses have almost the same orientation (4.49° for O_1 and 0.09° for K_1). Hence, we would expect a more stratified water column before 2010. This is in good agreement with Souza and Simpson (1996). They observed that the stratification has an influence on the ellipse orientation: when the water column is mixed the surface and the bottom ellipses are oriented in the same direction (within 5°), but, when the water column stability develops, there is a bottom surface orientation difference of up to 15° with the bottom maximum current being deflected to the west relative to the surface currents.

Summarizing, in 2010-2014 we found a more homogenous benthic layer shown both from the water column thermohaline properties (CTD, and mooring data) and from the characteristics of the ellipse orientation at different depths. Then, we observed a change in the tidal ellipse orientations from parallel to the main DT axis to perpendicular to it. In addition, we detected a weaker bottom tide KE and EKE, together with a much smaller current shear.

In the previous section we observed that the tidal currents in the North-west Ross Sea are principally diurnal and according to Padman et al. (2009) and Robertson (2005) they are associated over the outer shelf and upper slope with diurnal, topographically trapped vorticity waves (DTVWs). See Huthnance (1978), Brink (1991) and Middleton et al (1987) for a summary of the properties of these waves.

According to Huthnance (1989), increasing the stratification will increase the wave speed and induce the frequency to increase. Furthermore, a modest change in slope or stratification can alter the DTVWs dispersion curves (Padman et al., 2009). In particular, according to Cummins et al. (2000) with homogeneous water, the DTVWs propagate relatively slowly and attenuate over a shorter distance than in the stratified case.

Thus, we speculate that before 2010, in a more stratified water column, the DTVWs formed at the shelf break propagate more vigorously and southward compared to after 2010 when the more homogenous water column decreases the tide influence at the mooring location. Unfortunately we can only speculate on this hypothesis, with only one single mooring we do not have enough data to verify it. However, we hope to explore this question more fully with an eddy resolving resolution (1.5km) model of the Ross Sea circulation (Mack et al., this issue) where we plan to artificially freshen the mCDW (as done in Smith et al., 2014) and explore the effects of this on the tidal forcing at the DT entrance.

The more homogenous water column after 2010 may depend on the freshening of the mCDW observed by Jacobs and Giulivi (2010). The freshening is clear, and can also be seen in Figure 13 where there is an evident shift of mCDW core registered at 400 m towards lower salinity from 2006 to 2012.

In summary, we speculate that the freshening of mCDW alters the stratification over the outer shelf influencing the tide that causes the change of the temperature oscillation before and after 2010.

The change of the observed temperature variability after 2010 may be related to the movement of the mooring in the different surveys. In 2010 and in 2012 the moorings were deployed slightly west compared to previous years. For example, in 2012 the mooring was located 2.1 km west of the one deployed in 2006. The maximum distance between two moorings deployed in all the campaigns is about 3.1 km and it is between the 2010 and 2004 moorings.

However, we reject this hypothesis. Firstly because, as we have shown in Figure 4, the mooring is located between two cores of mCDW with a sharp temperature gradient on both eastern and western sides of it, so moving the mooring eastward or westward may have the same effect on the temperature fluctuation. In addition, in 2006 the sharpest lateral gradient near the bottom (where the mooring temperatures are measured) is on the west side of the mooring (unfortunately, the 2012 closest CTD profile to the west does not reach the bottom), consequently, moving the mooring westward, as occurred in 2010 and in 2012, we should have found a stronger oscillation in the time series, the opposite of what we actually observed (Figures 6 and 10).

Secondly, as we have shown before, the ellipse orientations of the main tidal constituents that govern the bottom dynamics have a larger zonal component after 2010 (normal to the DT main axis) meaning a more east-west tidal transport during those years. Consequently, we would expect, at least during spring tides, a stronger temperature signal amplitude in the 2010-2014 time series, but we actually found stronger oscillations before 2010.

5 Conclusions

Based on the results and discussion presented in the previous sections we can summarize the conclusion in the following points:

1) Previous works using both observational data (Kohut et al. 2013) and numerical models (Wang et al. 2013) suggested that mCDW intrudes onto the shelf mainly on the west slope of the Ross Sea banks. Instead we highlight the presence of two main cores of mCDW that intrude over the shelf.
2) Although our mooring is always located south of the ASF, the mechanism that brings mCDW from mid-depth to the bottom and the relative mixing with HSSW, is the tidal stirring (with a daily and a fortnightly variability). Thanks to tidal mixing that brings mCDW to the bottom we are able to analyze the temporal variability of the CDW intrusion, although we only have sensors at the bottom of the trough, and they are 50 km distance from the shelf break.
3) Thanks to a unique time series (10 years long) collected by a mooring located close to the shelf break, it has been possible to explore beyond the small scale temporal variability: the seasonality and the interannual variability of mCDW inflow over the shelf.
4) A strong seasonal variability of mCDW intrusions is clear. It appears that a strong incursion of mCDW occurs each austral summer around the end of December/beginning of January and a relatively weaker one around July.

5) We observe a strict relationship between the tide and temperature signal both at the small temporal scale and the seasonal time scale. We speculate that the seasonal intrusion of mCDW into the bottom layer is governed by the tides, but may be modulated by the wind fields too.
6) Besides a seasonal variability we found, also, an interannual variability. We detected large differences in the temperature oscillation before and after 2010. Probably, this variability is tide related too. Change in the tidal behavior is likely related to a modification of the stratification, going from a more stratified to a more homogenous water column.
7) The mechanism that changes the tide behavior in relation to the stratification is likely associated with the influence on the DTVWs of the stratification. In a homogenous water column, DTVWs propagate relatively slowly and attenuate over a shorter distance than in the stratified case. Thus, we speculate that before 2010 in a more stratified water column the DTVWs formed at the shelf break propagate more vigorously and southward compared to after 2010 when the more homogenous water column decreases the tide influence at the mooring location. The more homogenous water column after 2010 may depend on the freshening of mCDW observed by Jacobs and Giulivi (2010).

Finally, considering that we obtained these results using data collected by a single mooring, some questions remain. We believe we could address some of them using model simulations of the Ross Sea cross slope dynamics. In particular, the three main points that should be investigated are:

- The role played by the wind stress in the seasonal variability by means of re-analysis and model experiment.

- The influence of the stratification on the DTVW dynamics and the role played by the DTVWs in the CDW inflow variability.
- The possible effect of the movement of the mooring on the observed variability in the tidal ellipses orientation.

Acknowledgments

This study was performed using the CLIMA, T-Rex and MORSea data sets. Logistical and financial support for these projects were provided by the Italian National Program for Antarctic Research (PNRA). We thank the CLIMA IV, T-Rex and MORSea teams and the crew of the RV Italica who provided excellent support during the field operations. Part of this research was co-funded by CONISMA (COnsorzio Nazionale Interuniversitario per le Scienze del MAre). The atmospheric re-analysis data were supplied by European Centre for Medium-range Weather Forecast.

References

Budillon, G., Pacciaroni, M., Cozzi, S., Rivaro, P., Catalano, G., Ianni, C., & Cantoni, C. (2003). An optimum multiparameter mixing analysis of the shelf waters in the Ross Sea. Antarctic Science, 15(1), 105–118. doi:10.1017/S095410200300110X

Budillon, G., Castagno, P., Aliani, S., Spezie, G., & Padman, L. (2011). Thermohaline variability and Antarctic bottom water formation at the Ross Sea shelf break. Deep Sea Research Part I: Oceanographic Research Papers, 58(10), 1002–1018. doi:10.1016/j.dsr.2011.07.002.

Burrus, C.S., Gopinath, R.A., Guo, H., (1998). Introduction to Wavelets and Wavelet Transforms, A Primer. Prentice Hall, Upper Saddle River, NJ (USA).

Brink, K. H., (1991). Coastal-trapped waves and wind-driven currents over the continental shelf. Annu. Rev. Fluid Mech., 23, 389– 412.

Cummins, P. F., Masson, D., & Foreman, M. G. G. (2000). Stratification and Mean Flow Effects on Diurnal Tidal Currents off Vancouver Island. Journal of Physical Oceanography, 30, 15–30.

Dee, D. P., Uppala, S. M., Simmons, a. J., Berrisford, P., Poli, P., Kobayashi, S., … Vitart, F. (2011). The ERA-Interim reanalysis: Configuration and performance of the data assimilation system. Quarterly Journal of the Royal Meteorological Society, 137(656), 553–597. doi:10.1002/qj.828

Dinniman, M. S., Klinck, J. M., & Smith, W. O. (2003). Cross-shelf exchange in a model of the Ross Sea circulation and biogeochemistry. Deep Sea Research Part II: Topical Studies in Oceanography, 50(22-26), 3103–3120. doi:10.1016/j.dsr2.2003.07.011.

Dinniman, M.S., J.M. Klinck, and W.O. Smith, Jr. (2011). A model study of Circumpolar Deep Water on the West Antarctic Peninsula and Ross Sea continental shelves. Deep-Sea Res. II, 58, 1508-1523.

Foreman, M.G.G., 1978. Manual for tidal currents analysis and prediction. Pacific Marine Science Report. 78-6. Institute of Ocean Sciences, Patricia Bay. 57 pp.

Foster, T. D., and E. C. Carmack (1976). Frontal zone mixing and Antarctic Bottom Water formation in the southern Weddell Sea, Deep Sea Res. Oceanogr. Abstr., 23(4), 301–317, doi:10.1016/0011-7471(76)90872-X.

Foster, T. D., A. Foldvik, and J. H. Middleton (1987). Mixing and bottom water formation in the shelf break region of the southern Weddell Sea, Deep Sea Research. Part A, 34, 1771–1794.

Foufoula-Georgiou, E., Kumar, P., (1995). Wavelet in Geophysics. Academic Press 373.

Gill, A., (1973). Circulation and bottom water production in the Weddell Sea. Deep-Sea Res., 20, 111–140.

Gordon, A. L., Padman, L., & Bergamasco, A. (2009). Southern Ocean shelf slope exchange. Deep Sea Research Part II: Topical Studies in Oceanography, 56(13-14), 775–777. doi:10.1016/j.dsr2.2008.11.002.

Gordon, A. L., Huber, B. a, & Busecke, J. (2015). Bottom water export from the western Ross Sea, 2007 through 2010. doi:10.1002/2015GL064457.Received.

Grinsted, A., J. C. Moore, and S. Jevrejeba (2004). Application of the cross wavelet transform and wavelet coherence to geophysical time series, Nonlinear Processes Geophys., 11, 561–566

Huthnance, J, M., (1978). On coastal trapped waves: Analysis and numerical calculation by inverse iteration. Journal of Physical Oceanography., 8, 74–92.

Huthnance, J. M., (1989). Internal tides and waves near the continental shelf edge. Geophys. Astrophys. Fluid Dyn., 48, 81–106.

Jacobs, S.S. (1991). On the nature and significance of the Antarctic Slope Front. Mar. Chem., 35, 9-24.

Jacobs, S. S. (2004). Bottom water production and its links with the thermohaline circulation. Antarctic Science, 16(4), 427–437. doi:10.1017/S095410200400224X

Jacobs, S. S., & Giulivi, C. F. (2010). Large Multidecadal Salinity Trends near the Pacific–Antarctic Continental Margin. Journal of Climate, 23(17), 4508–4524. doi:10.1175/2010JCLI3284.1

Jackett, D.R., McDougall, T.J. (1997). A neutral density variable for the world's oceans. Journal of Physical Oceanography 27 (2), 237–263.

Johnson, G. C. (2008). Quantifying Antarctic Bottom Water and North Atlantic Deep Water volumes. Journal of Geophysical Research, 113(C5), C05027. doi:10.1029/2007JC004477

Kantha, L. H., C. A. and Clayson (2000). Numerical Models of Oceans and Oceanic Processes, Int. Geophys. Ser., vol. 66, Elsevier, New York.

Kohut, J., E. Hunter, and B. Huber (2013). Small-scale variability of the cross-shelf flow over the outer shelf of the Ross Sea. J. Geophys. Res., 188, 1863-1876, doit:10.1002/jgrc.20090.

Klinck, J. M., & Dinniman, M. S. (2010). Exchange across the shelf break at high southern latitudes. Ocean Science, 6(2), 513–524. doi:10.5194/os-6-513-2010

Mack, S.L., Dinniman, M.S., McGillicuddy, Jr., D.J., Sedwick, P.N., and Klinck, J.M. (2015). Dissolved iron transport pathways in the Ross Sea: Influence of tides and mesoscale eddies in a regional ocean model. Submitted to this issue.

Meyers, S.D., Keu, B.G., O'Brien, J., (1993). An introduction to wavelet analysis in oceanography and meteorology: with application to the dispersion of Yanai waves. Monthly Weather Review 121 (10), 2858–2866.

Middlleton, J. H., Foster, T. D., & Foldvik, A. (1987). Middletton_1987_Diurnal Shelf Waves in the Southern Weddell Sea.pdf. Journal of Physical Oceanography, 17, 784 – 791.

Morlet, J., Arens, G., Forgeau, I., Giard, D., (1982). Wave propagation and sampling theory. Geophysics 47, 203–236

Morlet, J., (1983). Sampling theory and wave propagation. Acoustic Signal/image Processing and recognition. In: Chen, C.H. (Ed.), NATO ASI Series, 1. Springer Verlag, pp. 233–261.

Muench, R.D., Padman, L., Gordon, A.L., Orsi, A.H.,(2009). Mixing of a dense water outflow from the Ross Sea, Antarctica: the contribution of tides. Journal of Marine Systems. doi:10.1016/j.jmarsys.2008.11.003.

Müller, M. (2012). The influence of changing stratification conditions on barotropic tidal transport and its implications for seasonal and secular changes of tides. Continental Shelf Research, 47, 107–118. doi:10.1016/j.csr.2012.07.003.

Nicholls, K. W., S. Østerhus, K. Makinson, T. Gammelsrød, and E. Fahrbach (2009). Ice-ocean processes over the continental shelf of the southern Weddell Sea, Antarctica: A review, Rev. Geophys., 47, RG3003, doi:10.1029/2007RG000250.

Orsi, a. H., Johnson, G. C., & Bullister, J. L. (1999). Circulation, mixing, and production of Antarctic Bottom Water. Progress in Oceanography, 43(1), 55–109. doi:10.1016/S0079-6611(99)00004-X

Orsi, A. H., & Bullister, J. L. (2002). On the total input of Antarctic waters to the deep ocean : A preliminary estimate from chlorofluorocarbon measurements, 107.

Orsi, A. H., & Wiederwohl, C. L. (2009). A recount of Ross Sea waters. Deep Sea Research Part II: Topical Studies in Oceanography, 56(13-14), 778–795. doi:10.1016/j.dsr2.2008.10.033

Padman, L., Howard, S. L., Orsi, A. H., & Muench, R. D. (2009). Tides of the northwestern Ross Sea and their impact on dense outflows of Antarctic Bottom Water. Deep Sea

Research Part II: Topical Studies in Oceanography, 56(13-14), 818–834. doi:10.1016/j.dsr2.2008.10.026

Pawlowicz, R., Beardsley, B., Lentz, S., 2002. Classical tidal harmonic analysis including error estimates in MATLAB using T TIDE. Computers & Geosciences 28, 929–937.

Pereira, A. F., A. Beckmann, and H. H. Hellmer (2002). Tidal mixing in the southern Weddell Sea: Results from a three-dimensional model, J. Phys. Oceanogr., 32(7), 2151–2170, doi:10.1175/1520-0485(2002)032<2151:TMITSW>2.0.CO;2.

Pritchard, H. D., S. R. M. Ligtenberg, H. A. Fricker, D. G. Vaughan, M. R. van den Broeke, and L. Padman (2012). Antarctic ice-sheet loss driven by basal melting of ice shelves, Nature, 484, 502–505, doi:10.1038/nature10968.

Rignot, E., and S. S. Jacobs (2002). Rapid bottom melting widespread near Antarctic ice sheet grounding lines, Science, 296(5575), 2020–2023, doi:10.1126/science.1070942.

Robertson, R. (2005). Baroclinic and barotropic tides in the Ross Sea. Antarctic Science, 17(1), 107–120. doi:10.1017/S0954102005002890.

Smith, Jr., W.O., Dinniman, M.S., Hofmann, E.E., and Klinck, J.M. (2014). The effects of changing winds and temperatures on the oceanography of the Ross Sea in the 21st century. Geophysical Research Letters, 41, 1624-1631, doi: 10.1002/2014GL059311.

Souza, a. J., & Simpson, J. H. (1996). The modification of tidal ellipses by stratification in the Rhine ROFI. Continental Shelf Research, 16(8), 997–1007. doi:10.1016/0278-4343(95)00042-9.

Stewart, A. L., & Thompson, A. F. (2015). Eddy-mediated transport of warm Circumpolar Deep Water across the Antarctic Shelf Break. Geophysical Research Letters, 42(2), 432–440. doi:10.1002/2014GL062281.1.

UNESCO (1983). The acquisition, calibration and analysis of CTD data. A report of SCOR WG 51. Technical Papers in Marine Science, pp. 54–59.

UNESCO (1988). Algorithms for Computation of Fundamental Properties of Seawater. Technical Papers in Marine Science, pp. 44–53.

Visbeck, M. (2001). Deep velocity profiling using lowered acoustic Doppler current profilers: bottom track and inverse solutions. Journal of Atmospheric and Oceanic Technology 19, 794–807.

Wang, Q., Danilov, S., Hellmer, H., Sidorenko, D., Schröter, J., & Jung, T. (2013). Enhanced cross-shelf exchange by tides in the western Ross Sea. Geophysical Research Letters, 40(21), 5735–5739. doi:10.1002/2013GL058207.

Whitworth, T., & Orsi, a. H. (2006). Antarctic Bottom Water production and export by tides in the Ross Sea. Geophysical Research Letters, 33(12), L12609. doi:10.1029/2006GL026357.

Figure and table captions

Online version (color) Figure 1: Map of the western Ross Sea with bottom topography in meters. The transects A and B discussed in the text are shown by the red lines. The blue diamond indicates the mooring position. Locations of geographic features discussed in the text are also indicated: Cape Adare (CA), Drygalski Trough (DT) and Mawson Bank (MB).

Printed version (black and white) Figure 1: Map of the western Ross Sea with bottom topography in meters. The transects A and B discussed in the text are shown by the black thick lines. The grey diamond indicates the mooring position. Locations of geographic features discussed in the text are also indicated: Cape Adare (CA), Drygalski Trough (DT) and Mawson Bank (MB). The color version of this figure is available online.

Figure 2: Operation periods for the mooring deployed in the middle of the Drygalski Trough discussed in the text. The different gray lines indicate the instrument type (see legend, upper right).

Figure 3: Vertical section looking northward across the Drygalski Trough close to the shelf break (see transect A in Fig. 1): (a) potential temperature θ (°C); (b) neutral density γ^n (kg m^{-3}); (c) salinity S; (d) dissolved oxygen DO (mg l^{-1}); and (e) LADCP velocity (m s^{-1}) for the component normal to the Shelf Break (u_x - positive values directed offshore). The color version of this figure is available online.

Figure 4: Vertical section across the Drygalski Trough at the mooring location (black triangle), about 50 km from the shelf break (see transect B in Fig. 1) of: (a) potential temperature θ (°C) for the 2006 oceanographic survey; (b) neutral density γ^n (kg m^{-3}) for the 2006 oceanographic survey; (c) potential temperature θ (°C) for the 2012 oceanographic survey; and (d) neutral density γ^n (kg m^{-3}) for the 2012 oceanographic survey. The color version of this figure is available online.

Figure 5: Hourly time series of (a) salinity with temperature (°C) color coded and (b) neutral density γ^n (kg m^{-3}) with temperature (°C) color coded, registered by the bottom instruments on the mooring in the middle of the Drygalski Trough (see Fig. 1 for location).

Figure 6: Hourly time series of the temperature (°C), registered by the bottom instruments (about 20 m above the bottom; in grey) and by the upper instrument (about 80 m above

the bottom; in black) on the mooring in the middle of the Drygalski Trough (see Fig. 1 for location).

Figure 7: Wavelet power spectrum for the 2012 - 2014 time series registered by the bottom sensors (about 20 m above the bottom), on the mooring in Fig. 1, of the (a) temperature (°C) (T); (b) zonal component (u, ms^{-1}) of the bottom current; (c) meridional component (u, ms^{-1}) of the bottom current; and (d) magnitude (V, ms^{-1}) of the bottom current meter. The significance level (thick black line, 95%) and the cone of influence (thin black line) are also indicated.

Figure 8: Potential temperature/salinity (θ/S) scatter plot of the (a) 2004 – 2005 time series; (b) 2005 – 2006 time series and (c) 2006 – 2007 time series. The blue horizontal line shows the surface freezing point of seawater.

Online version (color) Figure 9: three-months subsets from (a) February 2004; (b) November 2004; (c) February 2013; (d) November 2013; of (starting from the top): (first panel) the zonal component (u, m s^{-1}) differences between the upper and the bottom sensors (thick blue line), tidal component of u (thin black line); (second panel) meridional component (v, m s^{-1}) differences between the upper and the bottom sensors (thick blue line), tidal component of v (thin black line); (third panel) current velocity (V, m s^{-1}) differences between the upper and the bottom sensors (thick blue line), tidal component of V (thin black line), Eddy Kinetic Energy (EKE, J – thick red line) for the bottom sensors scaled for 2; (fourth panel) temperature (°C) registered by the bottom (thin black line) and upper (thin blue line) sensors.

Printed version (black and white) Figure 9: three-months subsets from (a) February 2004; (b) November 2004; (c) February 2013; (d) November 2013; of (starting from the top): (first panel) the zonal component (u, m s^{-1}) differences between the upper and the bottom sensors (thick grey line), tidal component of u (thin black line); (second panel) meridional component (v, m s^{-1}) differences between the upper and the bottom sensors (thick grey line), tidal component of v (thin black line); (third panel) current velocity (V, m s^{-1}) differences between the upper and the bottom sensors (thick grey line), tidal component of V (thin black line), Eddy Kinetic Energy (EKE, J – thick black line) for the bottom sensors scaled for 2; (fourth panel) temperature (°C) registered by the bottom (thick black line) and upper (thick grey line) sensors. The color version of this figure is available online.

Figure 10: low-pass filtered (with a cutoff of 15 days) time series of the (a) Eddy Kinetic Energy (EKE, J); (b) tidal kinetic Energy (Tide KE, J) and (c) temperature (°C) registered by the bottom sensors over the entire sampling period from January 2004 to January 2014.

Figure 11: Monthly average along shelf break wind component from 2004 to 2011 (see legend lower right for the different years) of the daily mean ERA-interim (ECMWF) time series. The data where averaged over the area close to the shelf break in the western Ross Sea (from 71.5° S to 72.5° S & from 172° E to 176° E). The along-shelf break wind component is obtained rotating the coordinate system by 26° so that one component roughly aligns with the Ross Sea shelf break line in the subset area.

Online version (color) Figure 12: Tidal ellipses of the main constituents O_1 (left panel) and K_1 (right panel) at different depths throughout the entire sampling period for the 2004 (left) and 2012 (right) mooring time series. The red dashed line indicates the direction of the Drygalski Trough main axis (about 36° N).

Printed version (black and white) Figure 12: Tidal ellipses of the main constituents O_1 (left panel) and K_1 (right panel) at different depths throughout the entire sampling period for the 2004 (left) and 2012 (right) mooring time series. The grey dashed line indicates the direction of the Drygalski Trough main axis (about 36° N). The color version of this figure is available online.

Figure 13: Potential temperature/salinity (θ/S) scatter plot of the transect B (see Figures 1 and 4), color coded by the longitude (°E), for the (a) 2006 oceanographic survey and (b) 2012 oceanographic survey. The blue horizontal line shows the surface freezing point of seawater. The color version of this figure is available online.

Table 1: tidal Parameters, computed using T_tide, for the single instruments for each survey: tide constituent frequency (Freq, cycles/hour), major and minor axis (U_{maj} U_{min}, cm s^{-1}), tidal ellipse inclination (Inc, °N) and phase to the Greenwich meridian (pha, °)

Figure(s)
Click here to download Figure(s): Figure_1_color.eps

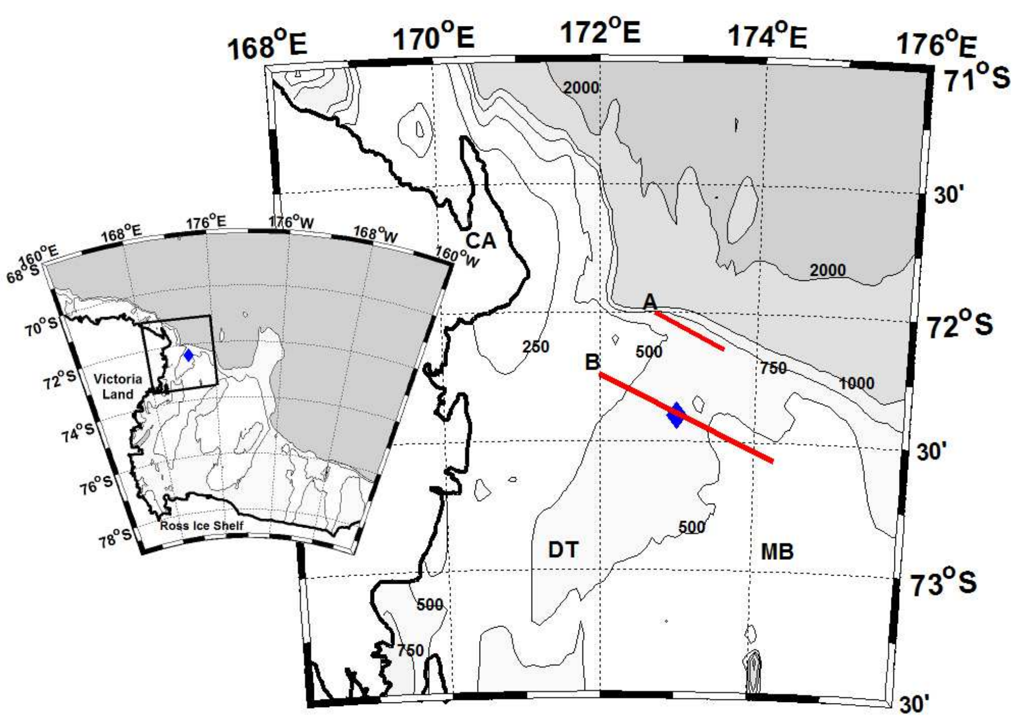

Figure(s)
Click here to download Figure(s): Figure_1_BW.eps

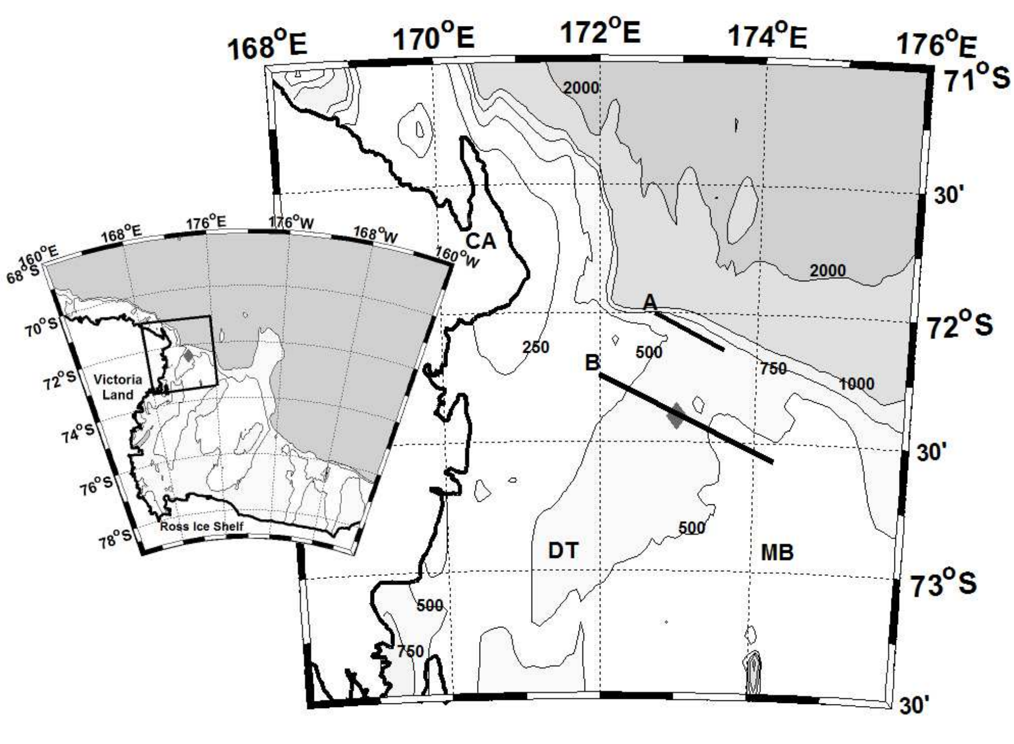

Figure(s)
Click here to download Figure(s): Figure_2.eps

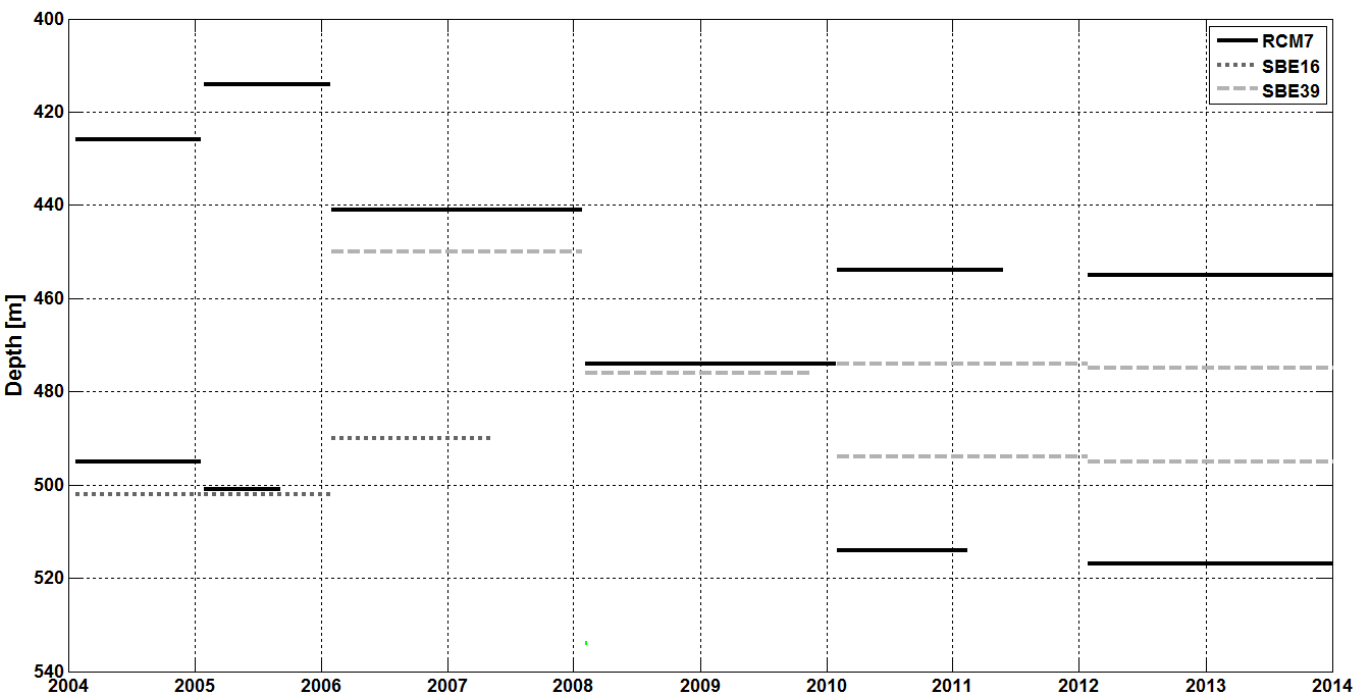

Figure(s)
Click here to download Figure(s): Figure_3_color.eps

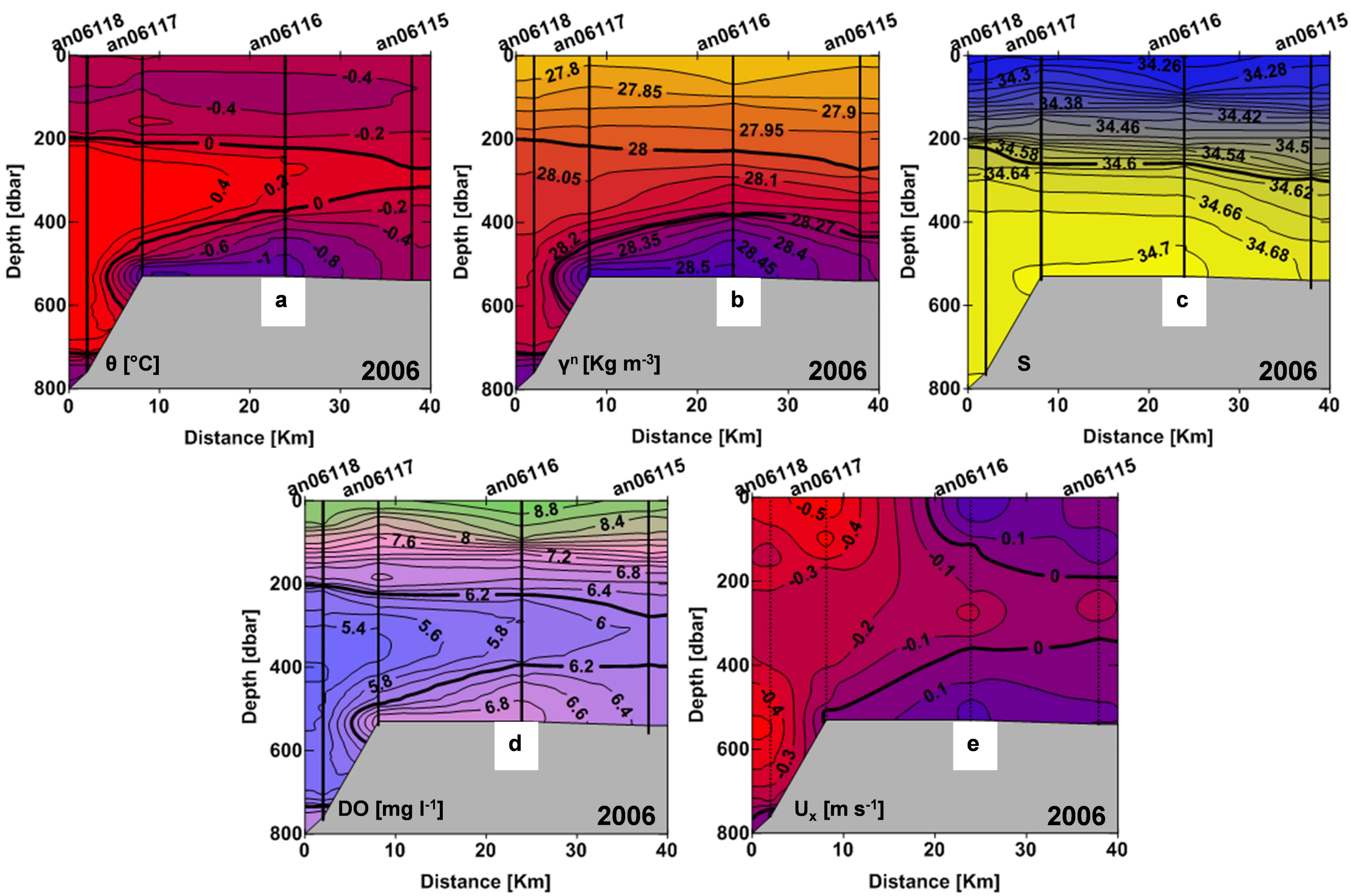

Figure(s)

Click here to download Figure(s): Figure_3_BW.eps

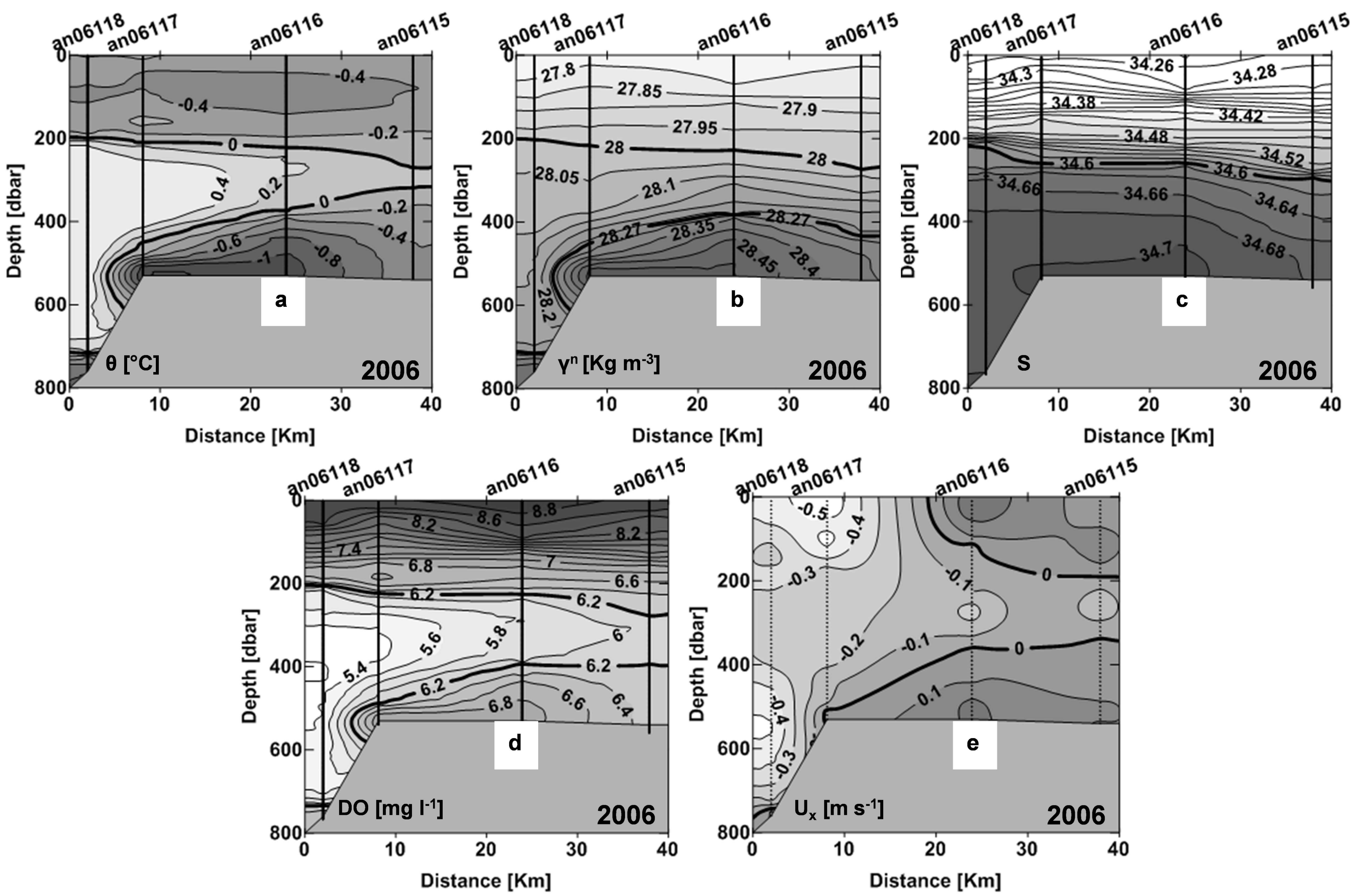

Figure(s)

Click here to download Figure(s): Figure_4_color.eps

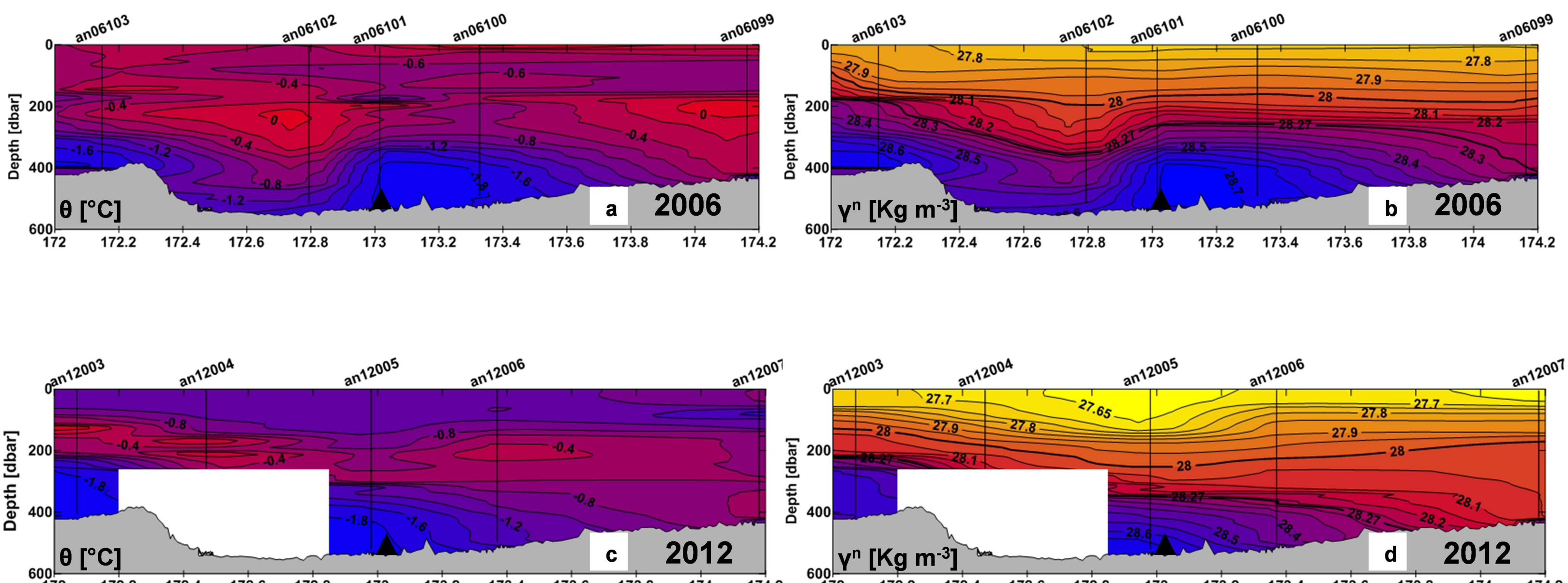

Figure(s)

Click here to download Figure(s): Figure_4_BW.eps

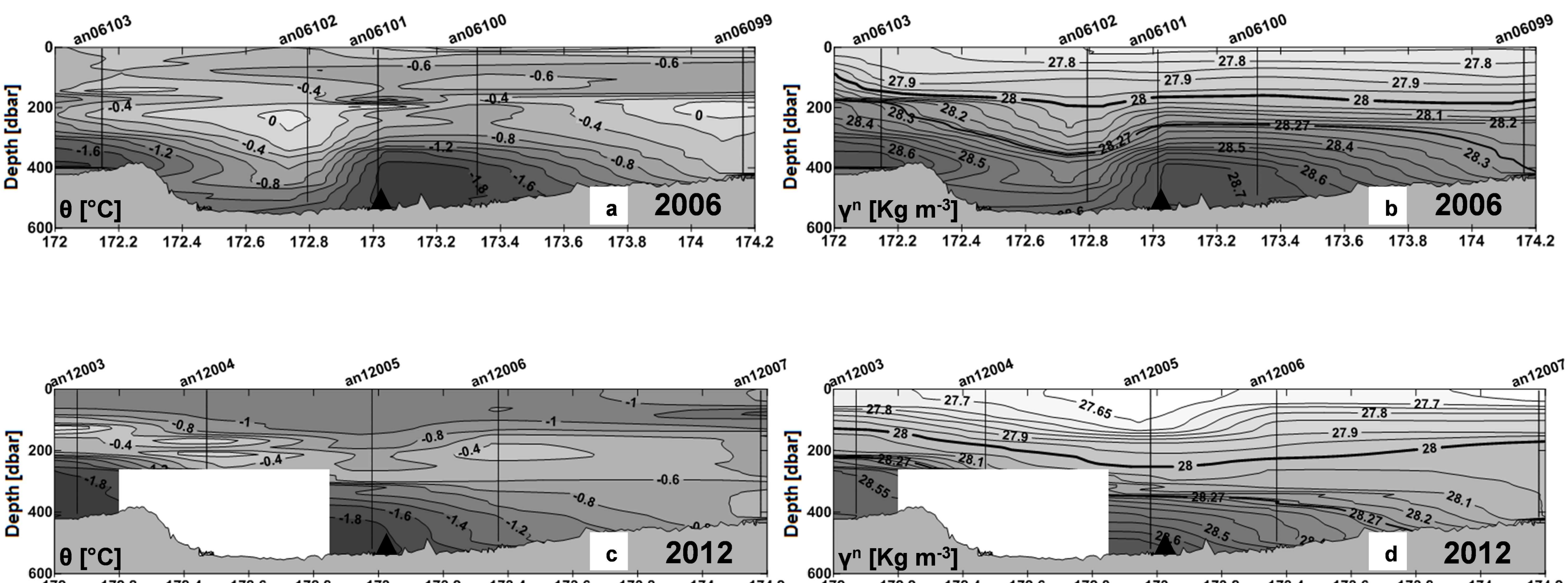

Figure(s)
Click here to download Figure(s): Figure_5.eps

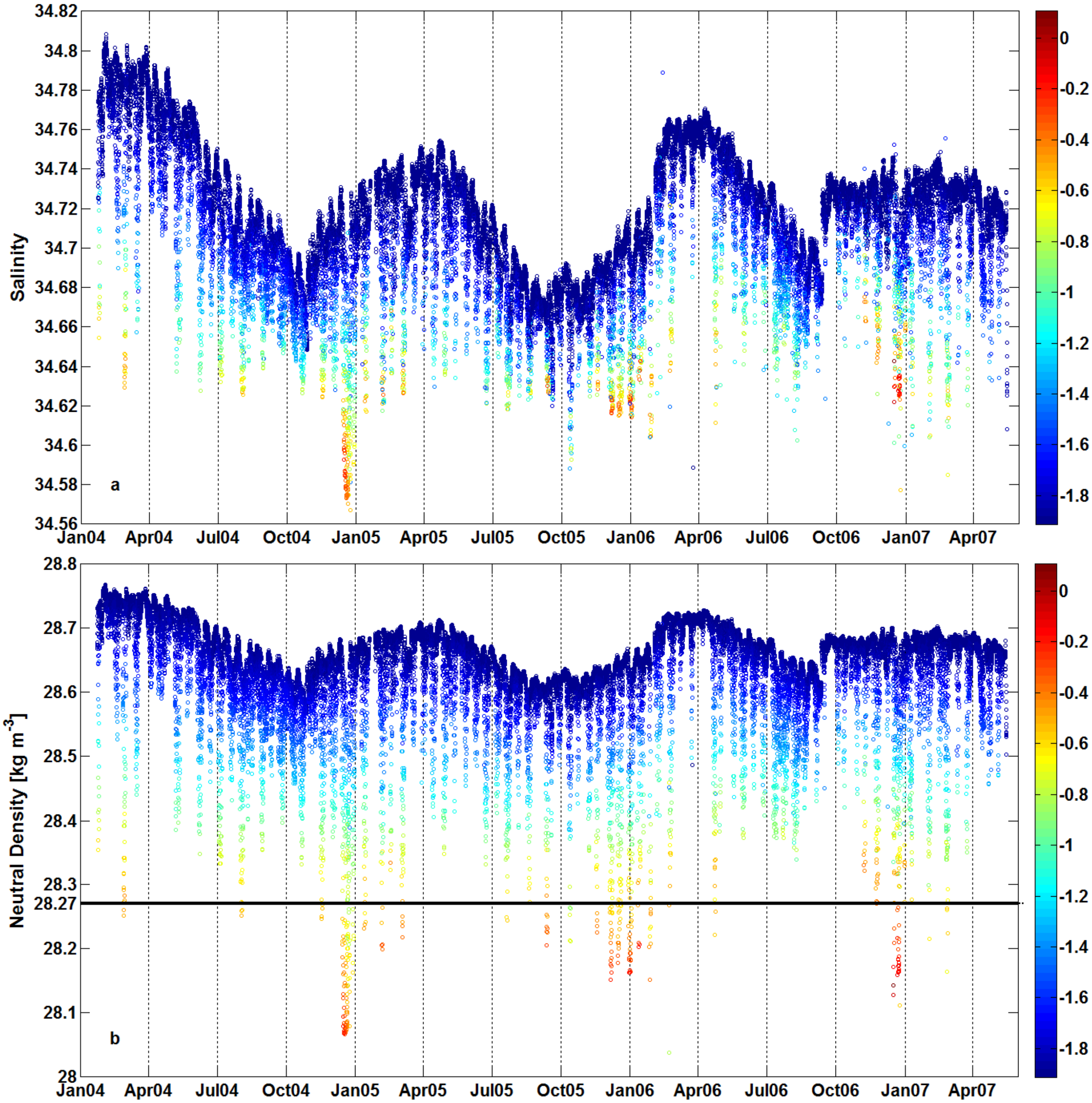

Figure(s)
Click here to download Figure(s): Figure_6.eps

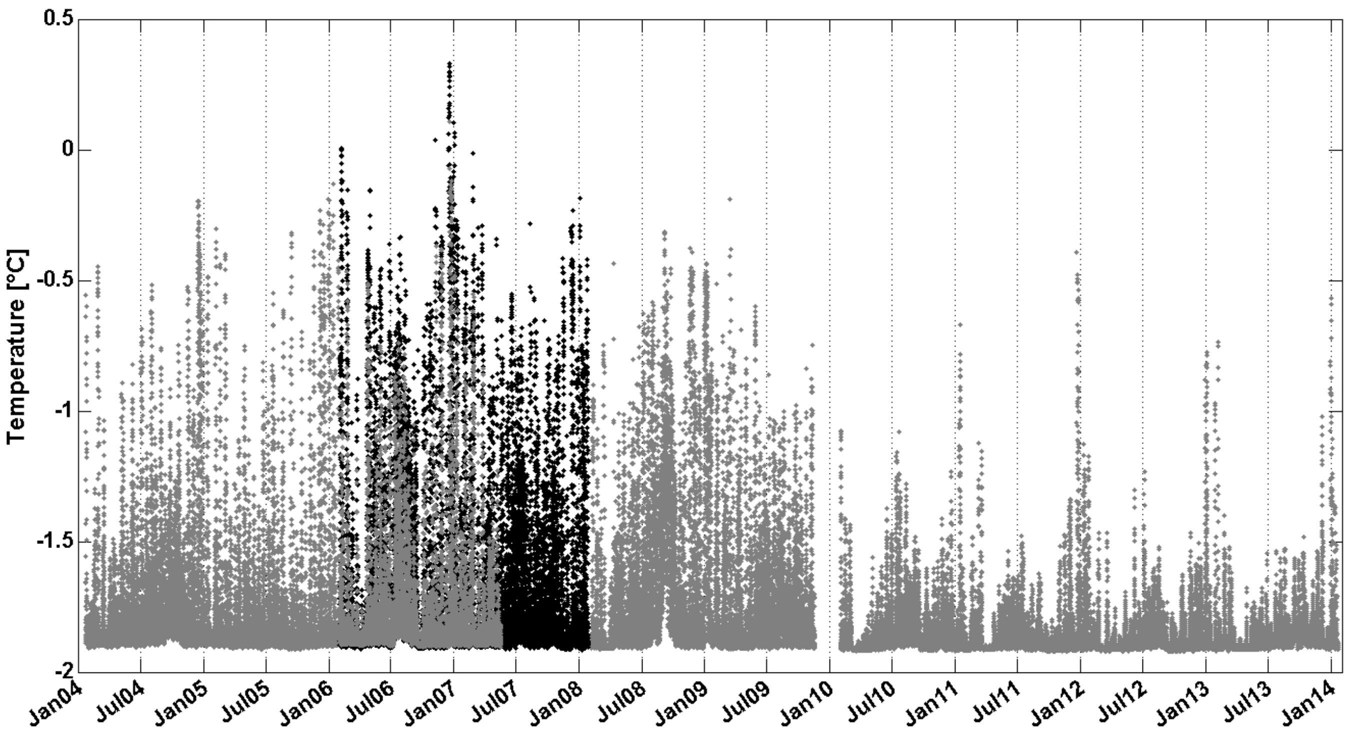

Figure(s)

Click here to download Figure(s): Figure_7.eps

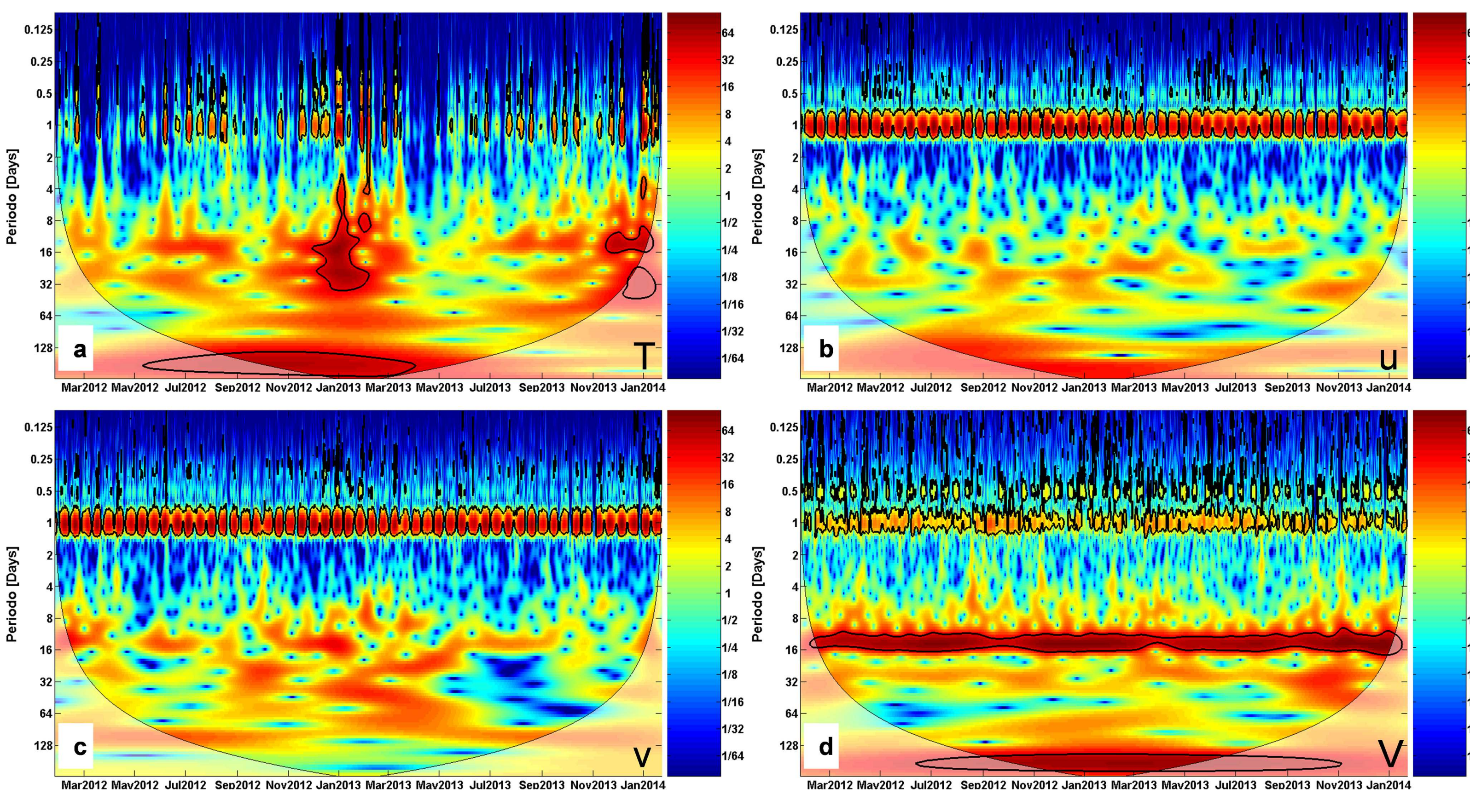

Figure(s)
Click here to download Figure(s): Figure_8.eps

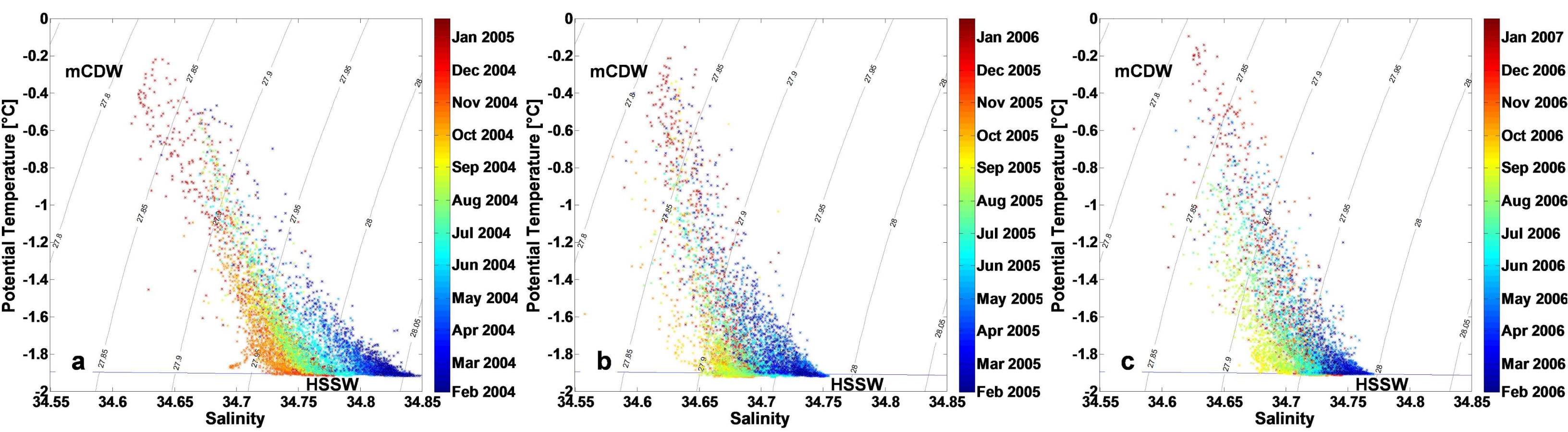

Figure(s)
Click here to download Figure(s): Figure_9a_color.eps

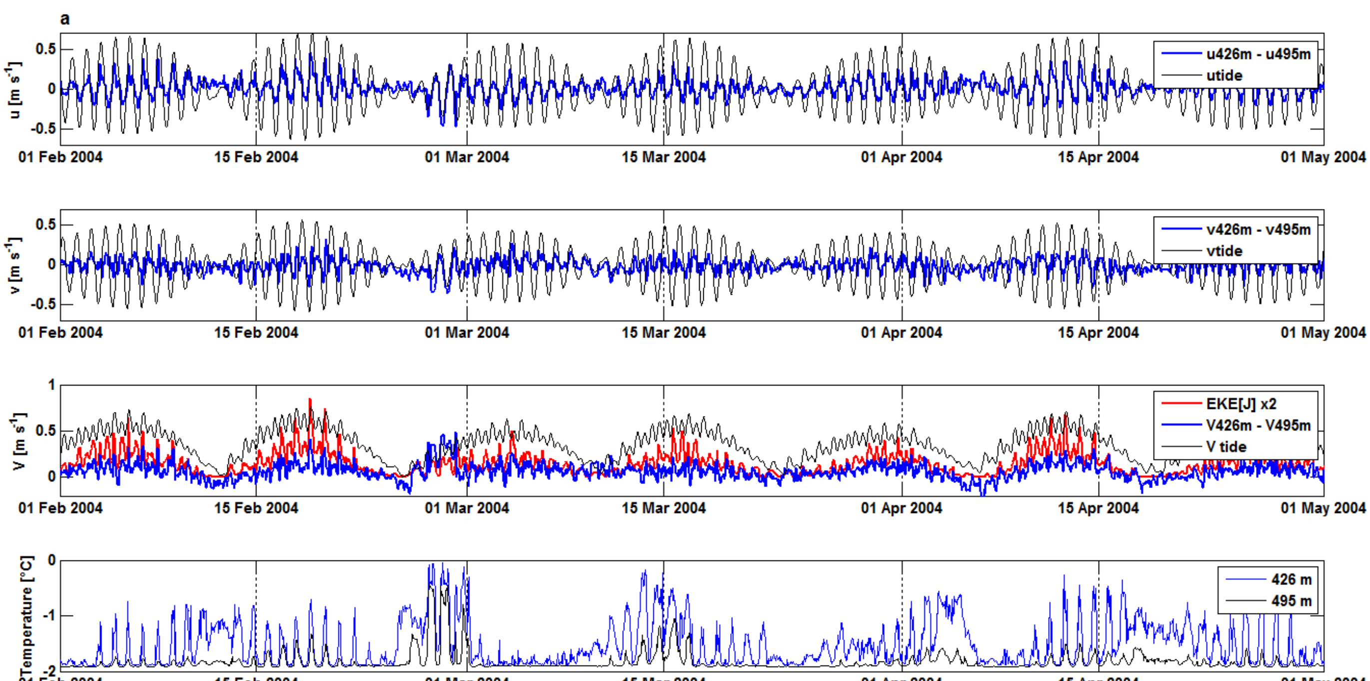

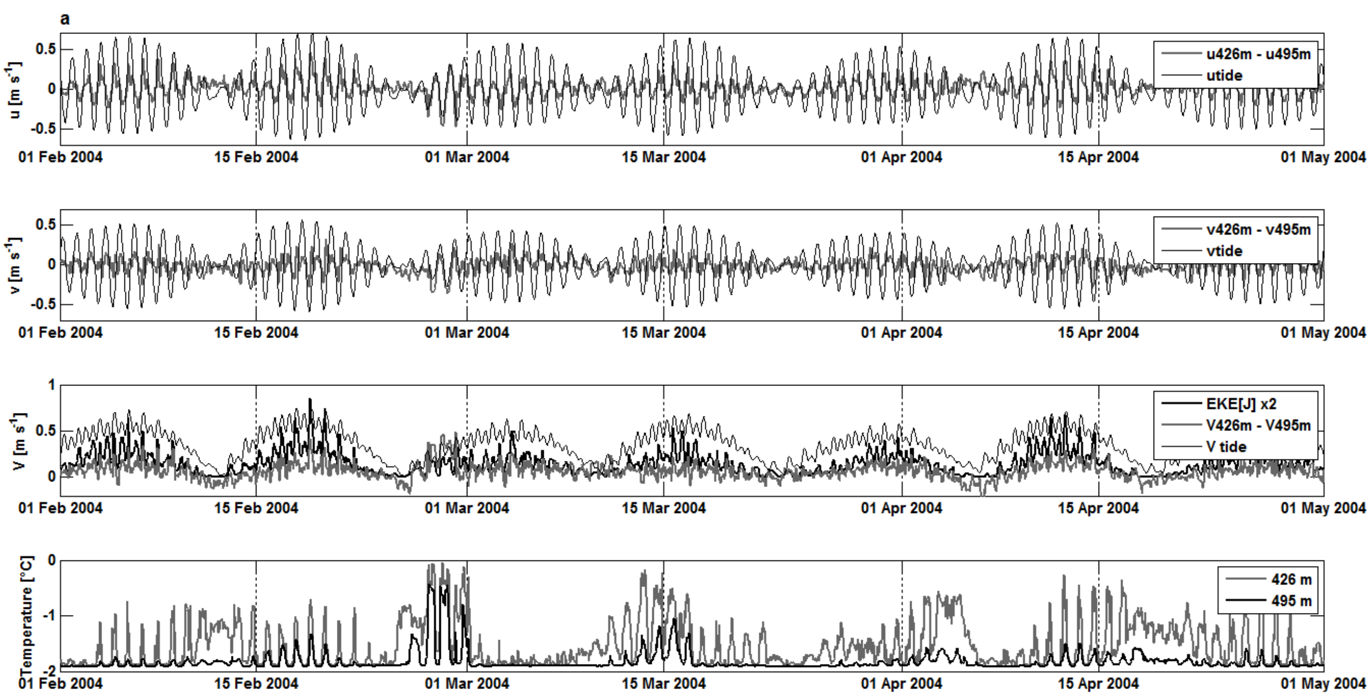
a
u [m s^{-1}]
0.5
0
-0.5
u426m - u495m
utide
v [m s^{-1}]
v426m - v495m
vtide
V [m s^{-1}]
1
EKE[J] x2
V426m - V495m
V tide
Temperature [°C]
-1
-2
426 m
495 m
01 Feb 2004
15 Feb 2004
01 Mar 2004
15 Mar 2004
01 Apr 2004
15 Apr 2004
01 May 2004

Figure(s)
Click here to download Figure(s): Figure_9b_color.eps

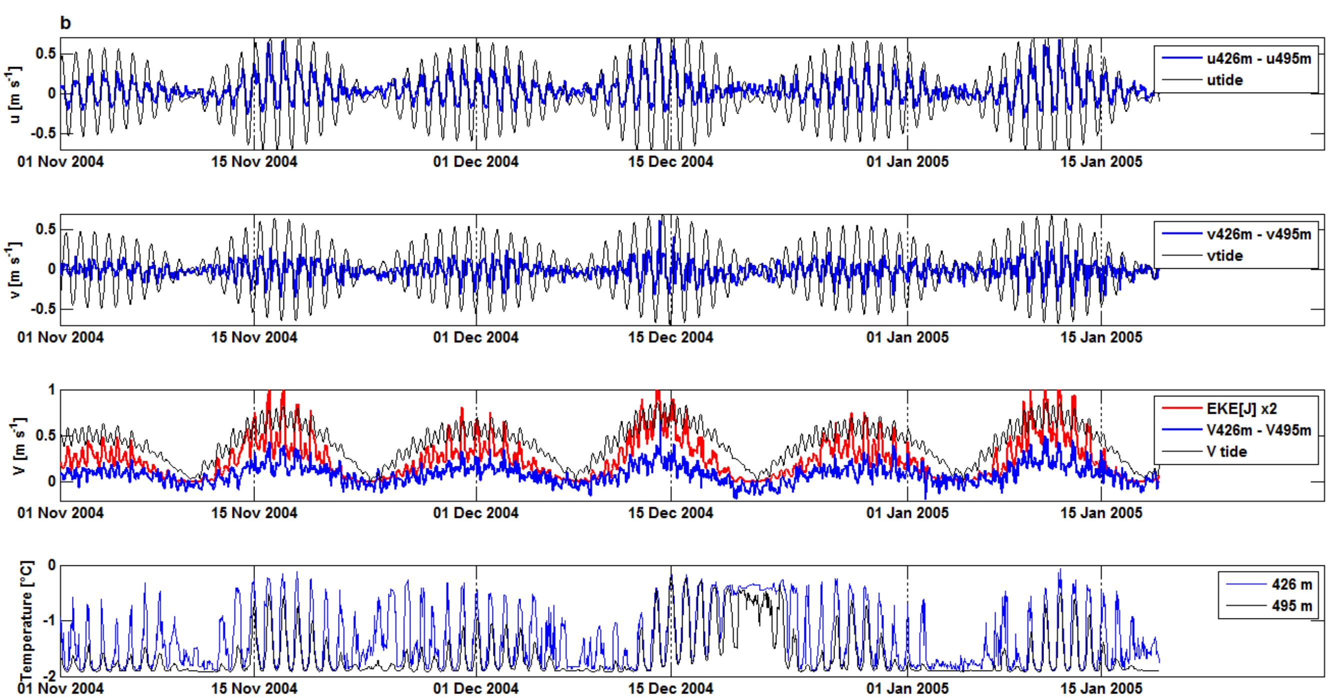

Figure(s)
Click here to download Figure(s): Figure_9b_BW.eps

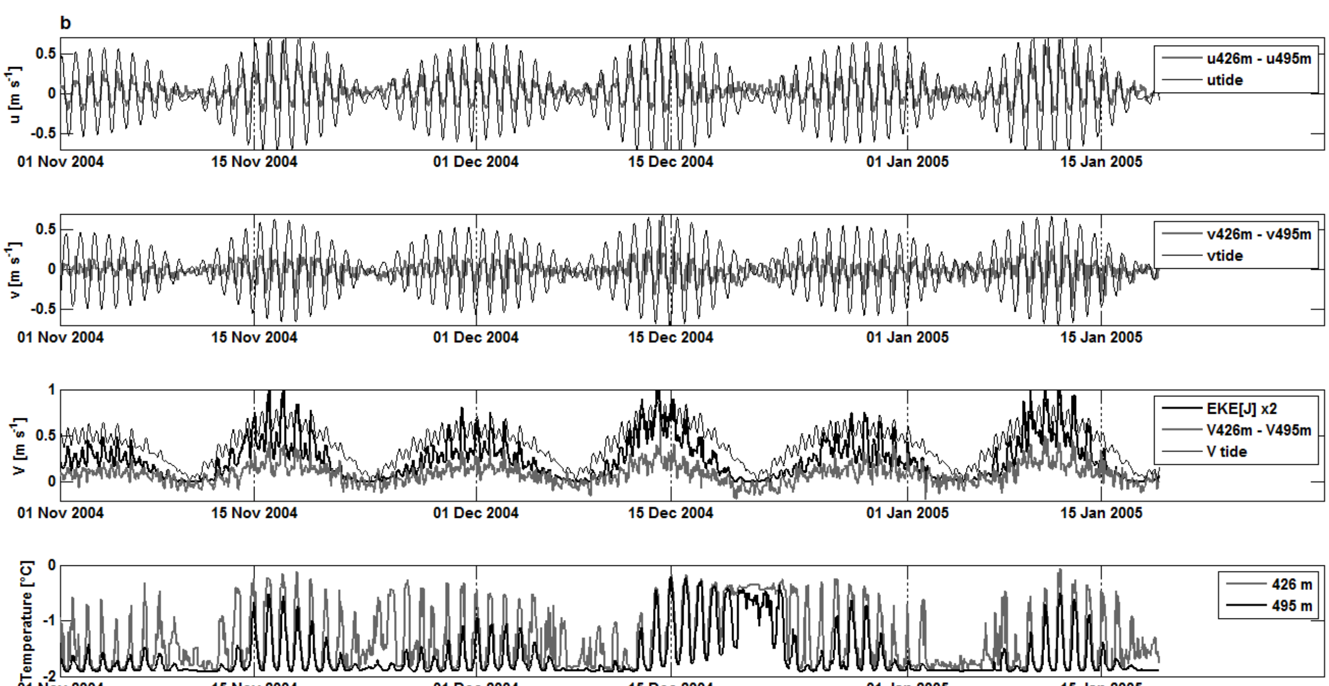

Figure(s)
Click here to download Figure(s): Figure_9c_color.eps

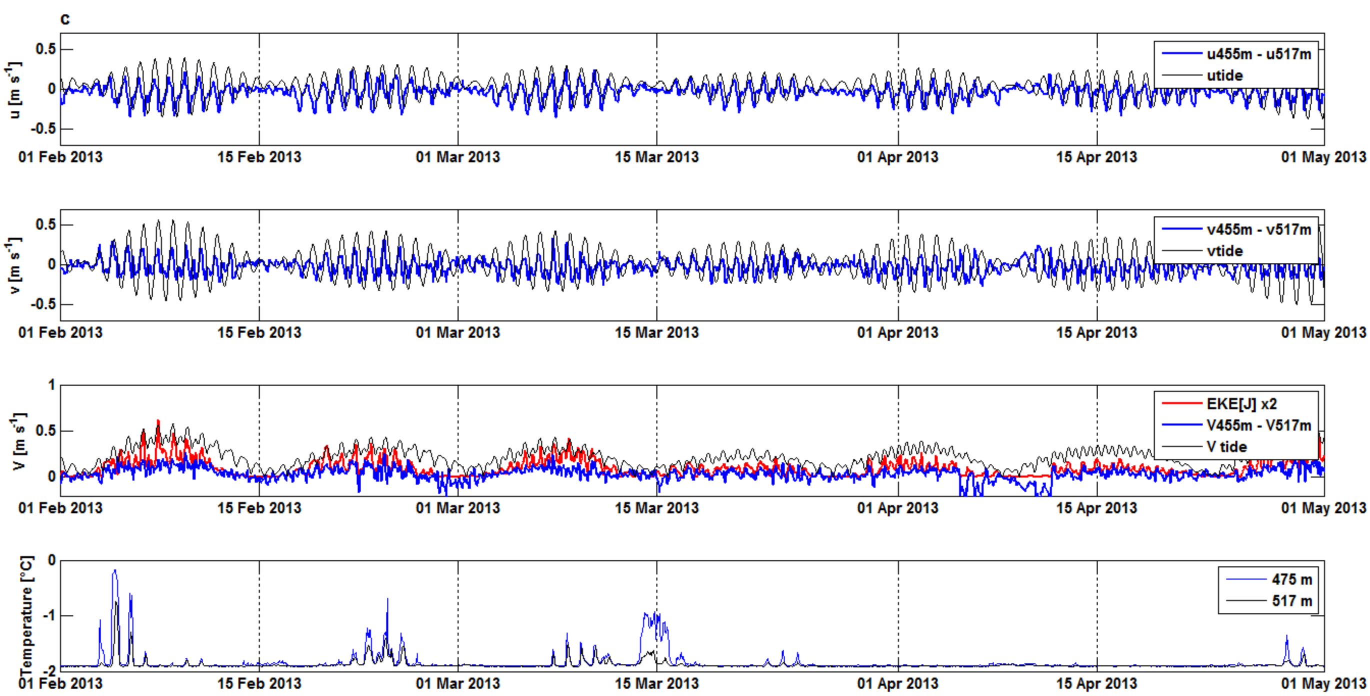

Figure(s)
Click here to download Figure(s): Figure_9c_BW.eps

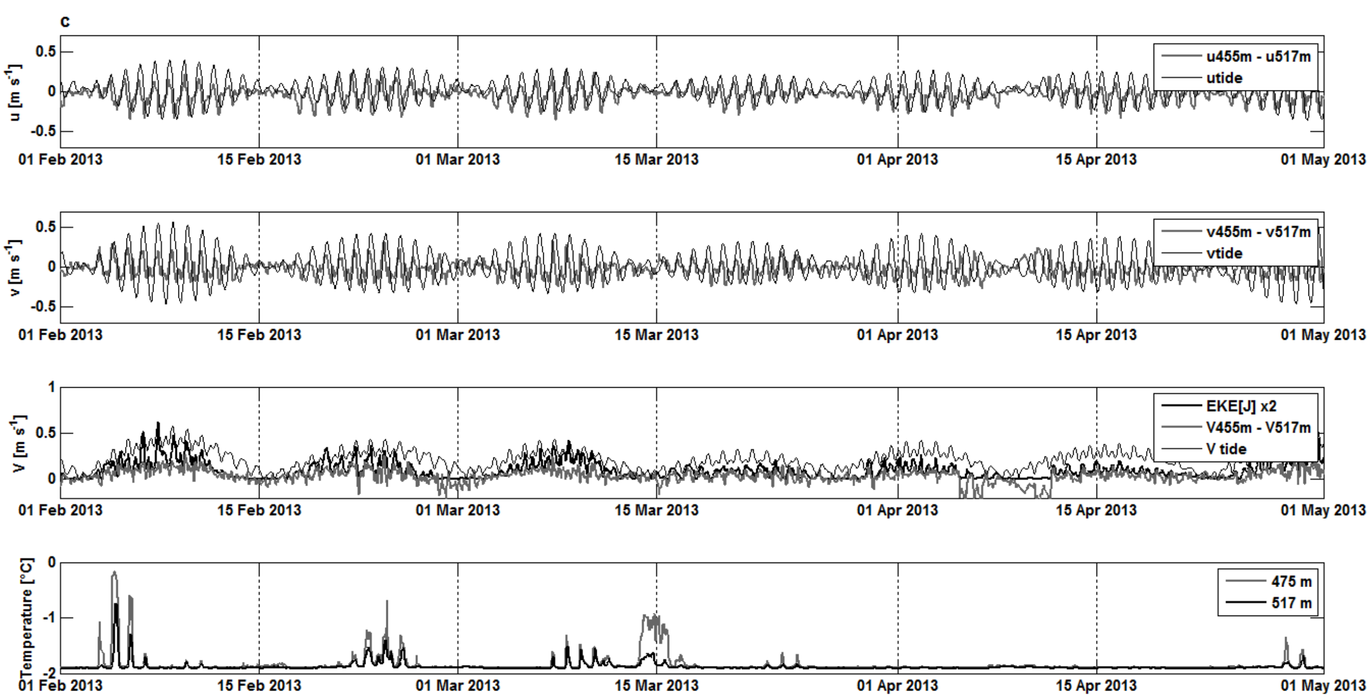

Figure(s)

Click here to download Figure(s): Figure_9d_color.eps

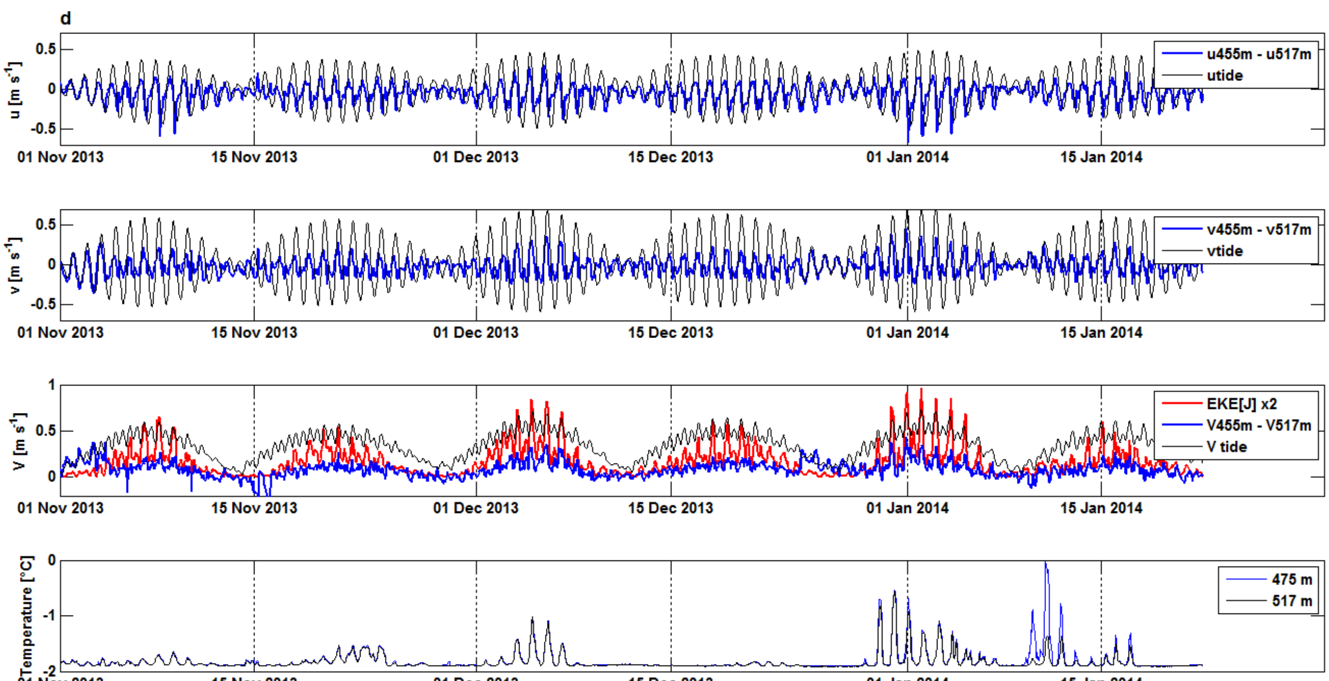

Figure(s)

Click here to download Figure(s): Figure_9d_BW.eps

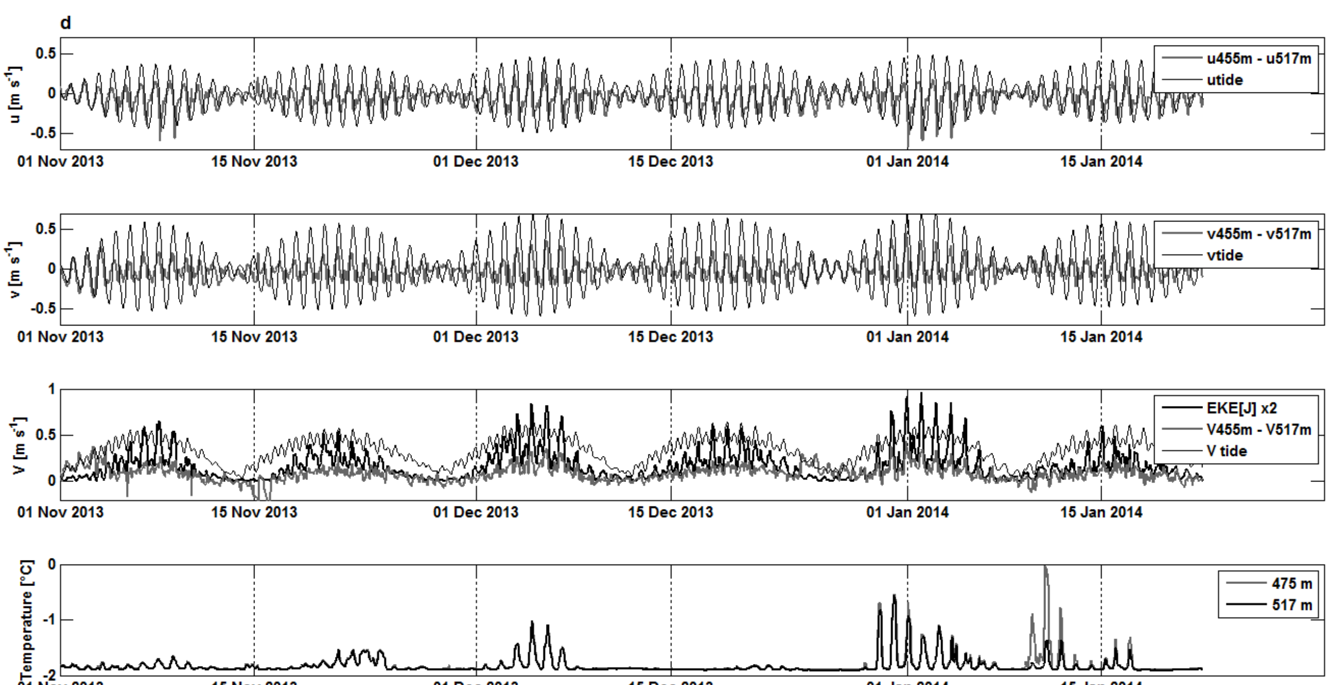

Figure(s)
Click here to download Figure(s): Figure_10.eps

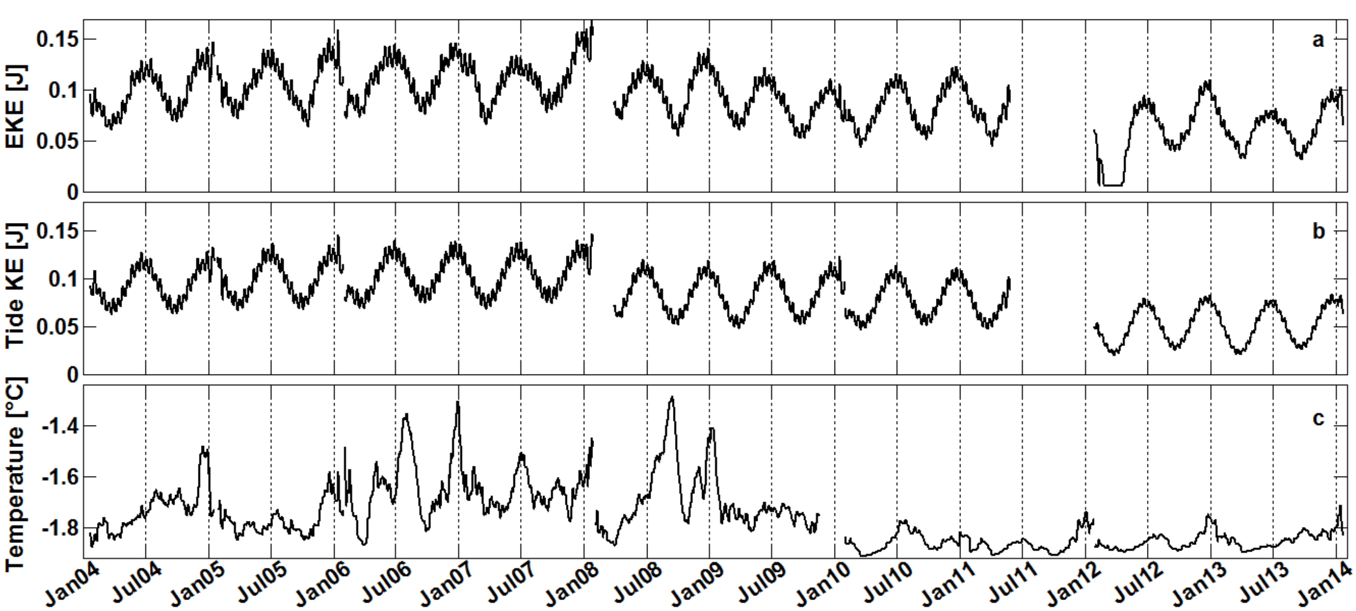

Figure(s)

Click here to download Figure(s): Figure_11.eps

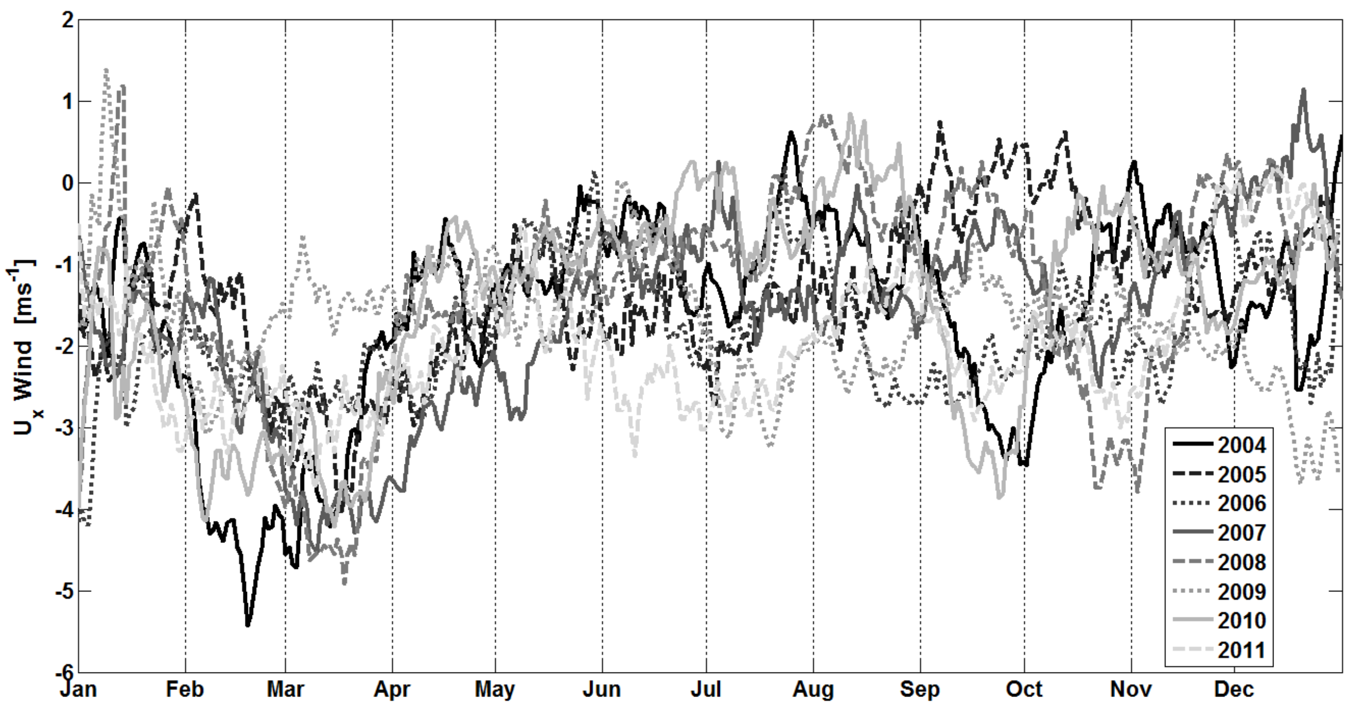

Figure(s)

Click here to download Figure(s): Figure_12_color.eps

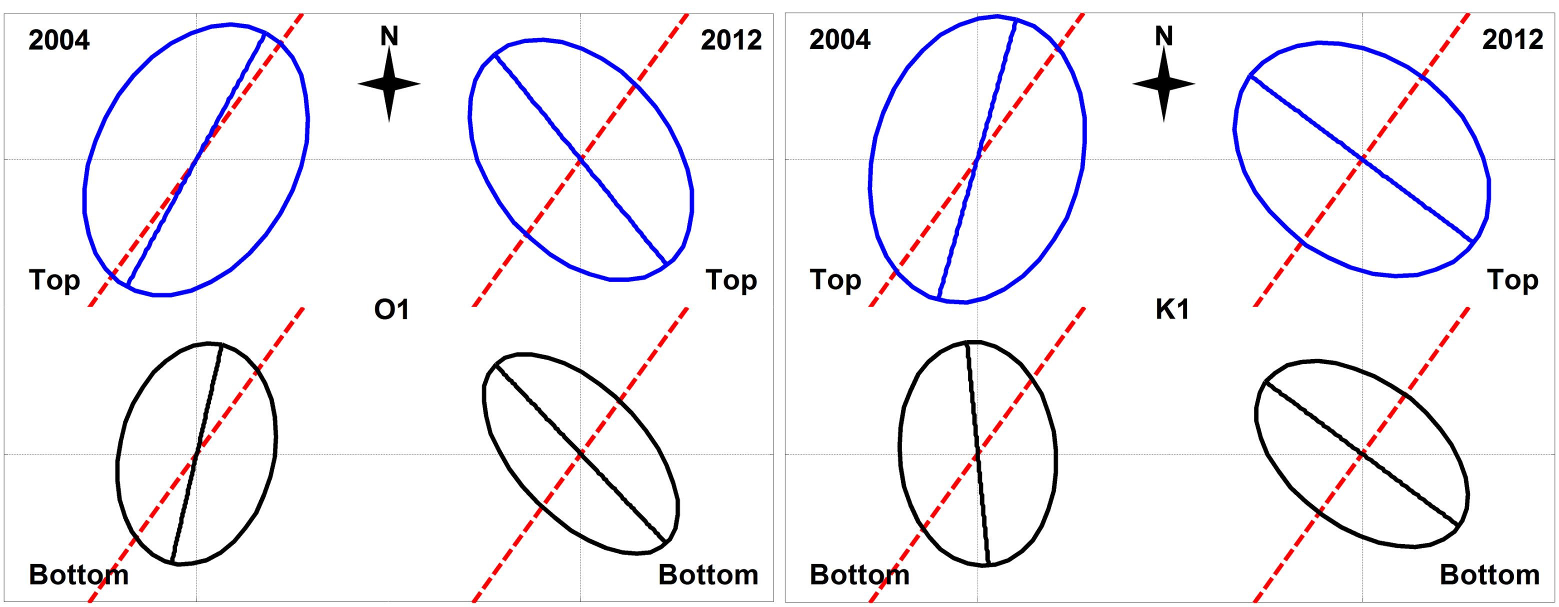

Figure(s)
Click here to download Figure(s): Figure_12_BW.eps

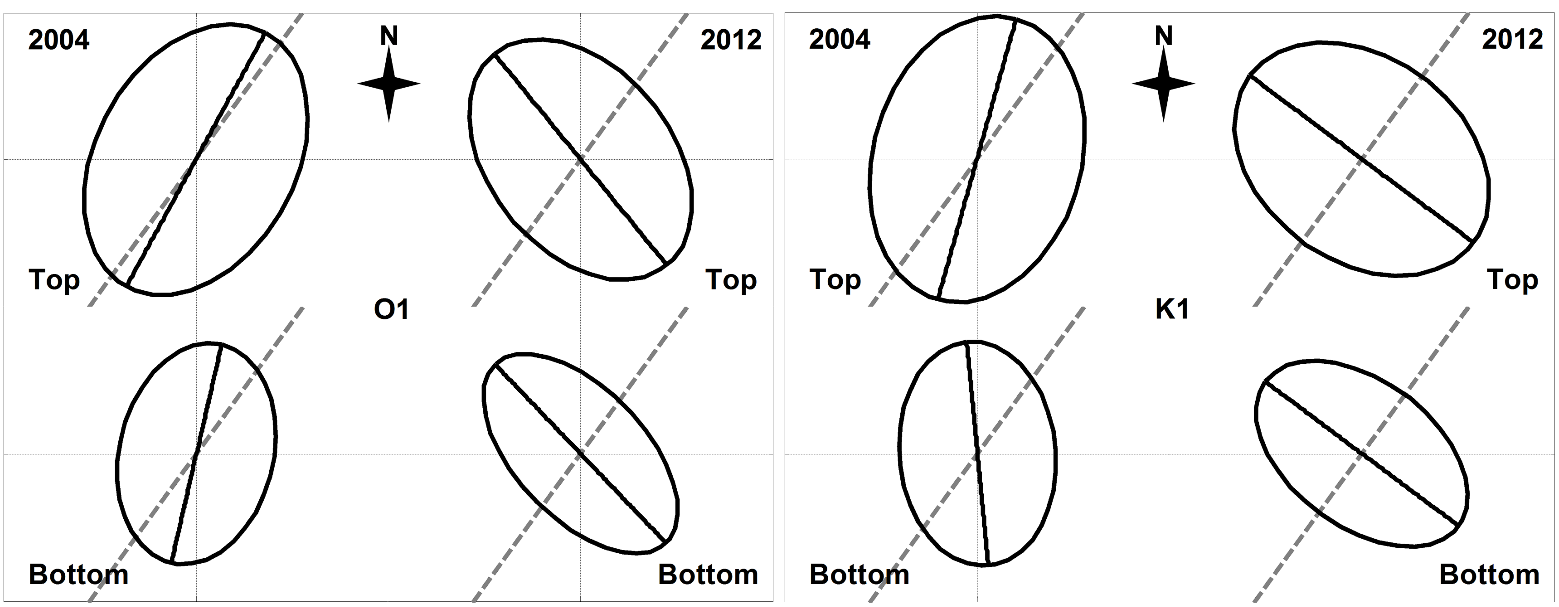

Figure(s)
Click here to download Figure(s): Figure_13_color.eps

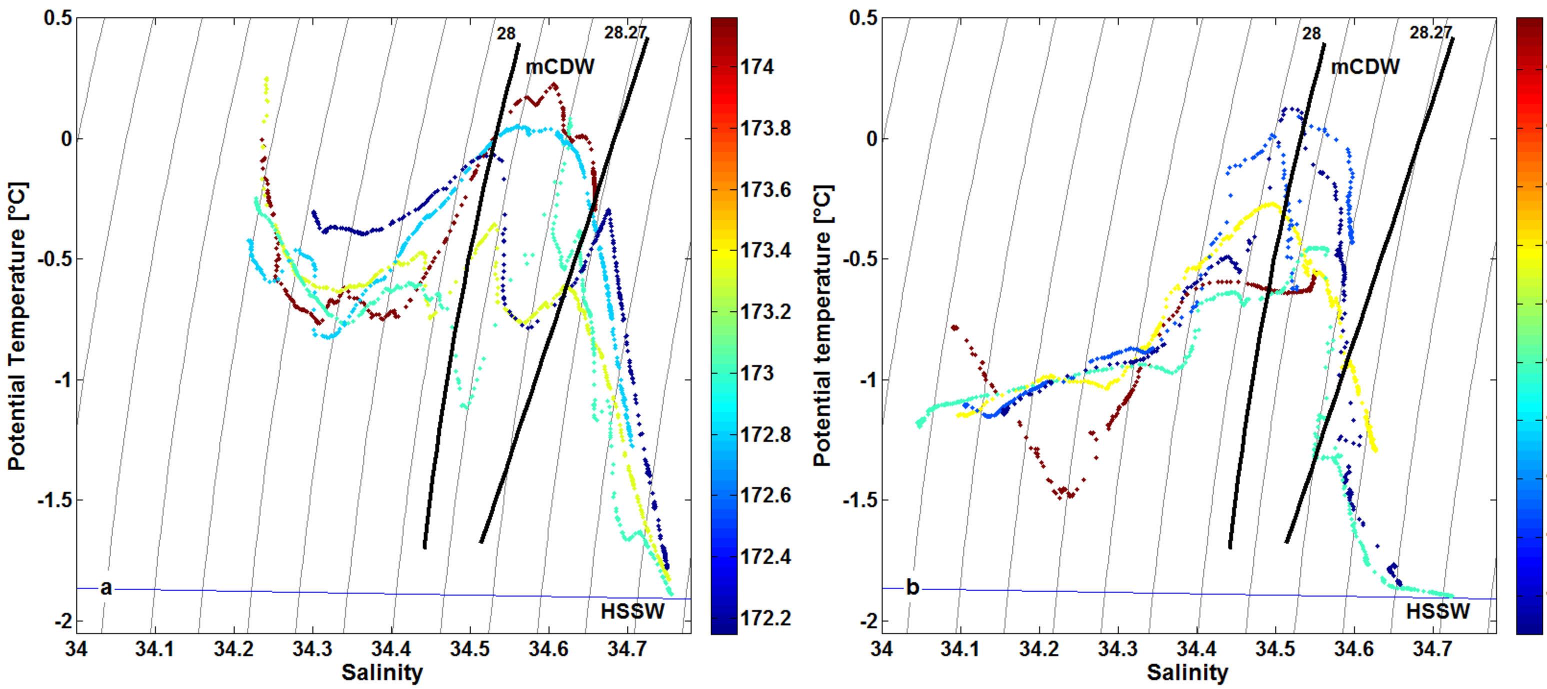

Figure(s)

Click here to download Figure(s): Figure_13_BW.eps

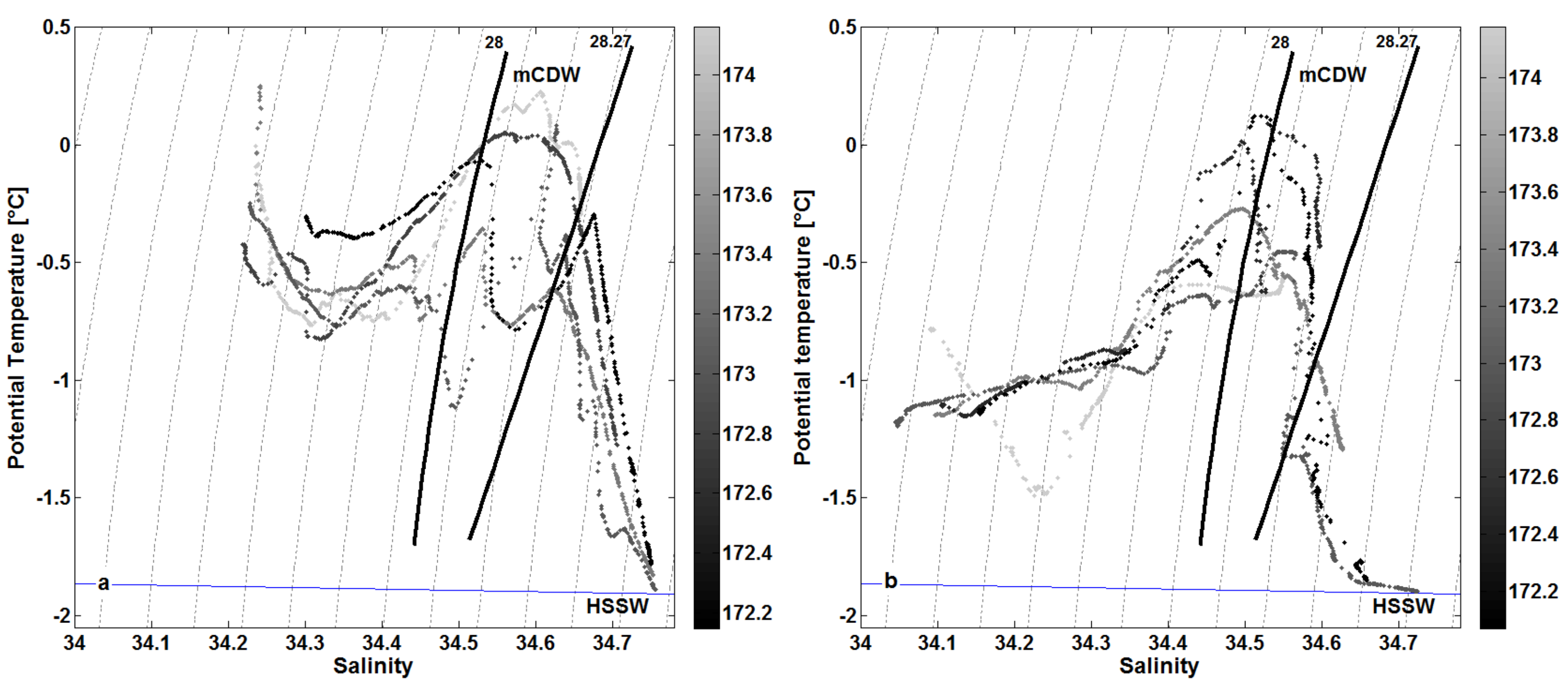

Table(s)

Click here to download Table(s): tables_I_Castagno_et_al_CDW_inflow_variability.docx

Deployment Year	Instrument Depth (m)	Tide	Freq (cph)	Umaj (ms^{-1})	Umin (ms^{-1})	Inc (°N)	Pha (°)
2004	426	MF	0.0031	0.048	-0.008	236.72	76.51
		Q1	0.0372	0.058	0.041	210.58	128.85
		O1	0.0387	0.301	0.208	208.72	135.03
		P1	0.0416	0.100	0.070	198.17	169.25
		K1	0.0418	0.303	0.217	195.58	168.32
		M2	0.0805	0.022	0.008	202.23	44.82
2004	495	MF	0.0031	0.026	0.001	193.23	86.15
		Q1	0.0372	0.042	0.029	192.25	114.64
		O1	0.0387	0.232	0.160	193.03	122.74
		P1	0.0416	0.075	0.050	175.27	147.98
		K1	0.0418	0.233	0.162	174.45	148.70
		M2	0.0805	0.045	0.024	147.75	73.28
2005	414	MF	0.0031	0.061	-0.007	241.55	63.35
		Q1	0.0372	0.060	0.036	206.26	86.82
		O1	0.0387	0.320	0.212	213.41	107.21
		P1	0.0416	0.104	0.075	194.23	129.17
		K1	0.0418	0.294	0.213	200.5	135.37
		M2	0.0805	0.052	0.044	192.14	10.03
2005	501	MF	0.0031	0.021	-0.005	236.26	99.00
		Q1	0.0372	0.045	0.030	202.71	99.91
		O1	0.0387	0.246	0.178	207.49	112.56
		P1	0.0416	0.083	0.055	170.66	116.22
		K1	0.0418	0.236	0.185	186.14	131.89
		M2	0.0805	0.053	0.044	157.15	25.27
2006	441	MF	0.0031	0.051	-0.011	248.06	176.36
		Q1	0.0372	0.068	0.039	217.72	269.21
		O1	0.0387	0.324	0.208	217.39	194.43
		P1	0.0416	0.104	0.071	206.06	334.64
		K1	0.0418	0.310	0.211	205.56	334.57
		M2	0.0805	0.047	0.039	190.84	299.92
2008	474	MF	0.0031	0.038	-0.003	220.38	73.37
		Q1	0.0372	0.056	0.033	207.88	190.07
		O1	0.0387	0.289	0.192	206.72	196.97
		P1	0.0416	0.110	0.071	196.23	233.56
		K1	0.0418	0.295	0.195	194.19	235.58
		M2	0.0805	0.038	0.021	160.31	235.80
2010	454	MF	0.0031	0.045	-0.008	167.95	232.85
		Q1	0.0372	0.055	0.032	144.87	152.42
		O1	0.0387	0.306	0.200	142.52	171.00
		P1	0.0416	0.101	0.071	133.01	219.91
		K1	0.0418	0.304	0.213	131.11	221.72
		M2	0.0805	0.025	0.020	113.67	352.02
2010	514	MF	0.0031	0.034	0.000	148.56	221.18
		Q1	0.0372	0.039	0.021	134.14	12.63
		O1	0.0387	0.230	0.134	135.16	25.17
		P1	0.0416	0.075	0.053	128.89	63.90
		K1	0.0418	0.225	0.153	123.16	62.15
		M2	0.0805	0.021	0.017	234.23	215.14
2012	455	MF	0.0031	0.034	-0.008	190.47	269.55
		Q1	0.0372	0.052	0.032	143.35	285.00
		O1	0.0387	0.284	0.190	140.79	148.24
		P1	0.0416	0.106	0.075	130.8	112.38
		K1	0.0418	0.290	0.212	126.68	232.34
		M2	0.0805	0.026	0.020	123.46	335.22
2012	517	MF	0.0031	0.033	-0.003	160.3	227.36
		Q1	0.0372	0.046	0.021	136.9	311.87
		O1	0.0387	0.256	0.135	136.3	327.66
		P1	0.0416	0.087	0.050	130.94	7.46
		K1	0.0418	0.250	0.151	126.77	4.58
		M2	0.0805	0.033	0.018	119.72	24.33